UNIVERSITÀ DEGLI STUDI DI MILANO
FACOLTÀ DI SCIENZE MATEMATICHE,
FISICHE E NATURALI

Corso di Laurea Triennale in Fisica

Joint determination of the strong coupling constant α_s and of the partonic structure of the nucleon.

Relatore Interno: Prof. S. Forte

Correlatore : Dott. J. Rojo

Tesi di Laurea di
Simone Lionetti
matr. 724668

Anno Accademico 2009-2010

Contents

General introduction

One of the most fascinating branches of physics is the chapter of this science which aims at understanding the features of the microscopic world. This field has led to many of the most fundamental discoveries that mankind has achieved throughout its history: let us think of how much knowing about molecules, atoms or electrons has changed life during the last century, in both its practical and speculative sides.

We could say that the first revolution in the direction of studying the structure of matter was made when the first microscope was used to see objects and processes which presented the observer with a new phenomenology. Nevertheless, ordinary microscopes and human eyes have an intrinsic limitation in their potential, just because of their use of visible light as a probe. Namely, the problem is that ordinary light waves are very small compared to the world as we are used to see it, but they become a mean of investigation far too approximate when studying equally small objects. This is the reason why it was necessary to find other probes with a resolution smaller than ordinary light wavelength, which could give information about the natural world with extreme spatial accuracy. A simple analogy can be made in order to understand this point better. Let us think of our microscopic object as a car, and imagine throwing balls at it from one side as an experiment to investigate the car's features. Even for a blind scientist who knows nothing of the car it would be possible, albeit obviously not easy, to build up the approximate shape of the car knowing the angles at which many basket balls are bounced off it. If our car is the image for an atom, claiming to study the atom with light waves would be quite like trying to understand the shape of the car with balls of the size of a small mountain. This whole picture has been drawn to recall that the primary function of particle accelerators is not very different from that of a microscope: they are meant to throw high-momentum particles (thus small-wavelength probes according to quantum mechanics) at objects, in order to understand the main features of the smallest known constituents of matter.

There is one more face of the problem that the example of the car can help us understand in simple terms. When the subnuclear particles, namely the proton and the neutron, were first observed, it was quite obvious to think about them as a whole, as much as it is natural to think of the car as a single object when we hit it with a basket ball. Of course, there were some hints for the presence of a substructure in the nucleon: the possibility of classificating particles in multiplets suggested some kind of internal regularity pattern, but few scientists ventured as far as thinking of the supposed constituents of observed particles as true physical objects. But the endless pursuit of knowledge which moves the human mind is never satisfied with a score, it always moves from results to new questions and to the search for answers. Technological improvements provided particle physicists with more refined tools for their work, that is higher-energy particles which could be used as precision probes for the objects they were studying. What took place can be compared to what would happen giving our imaginary scientist, who was throwing basket balls at the car, a gun. Firing bullets at the car and studying their angle of deflection would give him information not only about the shape of the object under examination, but also about its internal structure. As much as, given the gun, it is possible to distinguish the collision of a bullet with a rear mirror from that with a tyre, with deep inelastic scattering experiments it was possible for physicists to tell the difference between collisions of a probe with different parts of nucleon, which were later called partons.

Thanks to the many experiments which have been set up to investigate the deepest known nature of our world, the scientific world was able to develop a theory, called quantum chromodynamics, that actually allows calculations and interpretation of events which involve parton interactions. The main force involved in these processes is regarded as a fundamental interaction, goes by the name of strong coupling, and its actual strength is determined by a fundamental constant of nature associated to the symbol α_s. The aim of the present work is precisely to find a value of the strong coupling constant α_s, and the idea behind this determination is extremely simple. The value of the constant assumed to be correct is that which results in the best agreement among experimental data. More precisely, the constant is regarded as a free parameter and the object that measures data incompatibility, the chi square χ^2 according to the principle of least squares, is computed as a function of this parameter. Coherently with this principle we assume the value of α_s which gives the minimum χ^2 to be the best estimation for the fundamental constant, and by statistical arguments we are able to give boundaries to constrain it inside a well-defined interval. This operation will be conducted with caution, as the constant studied is extremely important for the determination of observable quantities in many experiments currently in progress, it has not a universally accepted value and there is not a common agreement about its experimental uncertainty yet.

This work is organized as follows. In chapter 1 the experimental and theoretical developments which have allowed today's model of the nucleon are summarized, in a brief overview that covers the fundamental concepts of quantum chromodynamics. The attention is focused on deep inelastic scattering experiments, which build up a great part of our data set, and on the determination of parton distribution functions, that is one of the aims of the present paper. Chapter 2 looks into the procedure chosen to obtain parton distribution functions, as well as in the empirical sources at the basis of our analysis. In the following section we discuss the strategy applied to obtain our estimation of the strong coupling constant and we assess the problem of interpolating a point set with strong random fluctuations independent for each datum. Last chapter deals with results for each considered experimental set, which we examine highlighting differences an studying procedural uncertainties.

Chapter 1

The Structure of the Nucleon

1.1 Deep Inelastic Scattering experiments

In the field of particle physics, most of the available empirical information comes from scattering experiments. The purpose of such physical experiences is to study the properties of particles through detailed analisys of their collisions. Practically speaking, there are two ways of obtaining this results: in fixed target experiments one beam of particles is accelerated and pointed against a target which is at rest in the laboratory frame, while in collider experiments two bunches of particles are both accelerated and later thrown one against the other. Though these two ways of setting up the experiment imply totally different problems concerning their realization and each has its advantages and disadvantages, there is no theoretical difference between the two as long as a change of frame is allowed. For the purpose of the following discussion, it is easier to think of these events in terms of a better known particle, the probe, that hits a fixed target whose properties are to be studied.

The first distinction that must be made is between elastic and inelastic processes. A collision is said to be elastic if the kinetic energy is conserved, meaning it is the same before and after the collision. Every time this does not happen and the system is actually isolated (this is nearly always the case in particle physics), we can deduce that some of the total energy of the system must have changed its shape, from kinetic energy to another form or vice versa. If at least one of the interacting particles is regarded as having some internal degree of freedom, it may be that some kinetic energy has passed from particle (translational) motion to this hidden store, changing the intrinsic status of the compound object. But if every particle involved is thought as truly elementary the only way to have a loss or an increase in total kinetic energy is particle formation or destruction.

Assuming that the initial state of the particles is perfectly known and given through their four-momenta, the final state is constrained by the total four-momentum conservation law, as there are no external forces acting on the system. Thus, of the initial eight degrees of freedom which characterize the situation after the collision (the eight components of the two four-vectors of the outgoing particles), only four free parameters remain. One of these is the scattering plane angle, which is not essential in order to understand the dynamics of the event. If we assume the probe to be an elementary particle, which is the case for our experiments where leptons are most commonly used because of their better-known interactions, the mass shell constrain on the outgoing probe gives another condition leaving only two free parameters. Usually the choice for these two quantities falls upon the energy loss of the probe and on the transferred square momentum, which has also an important physical interpretation being the norm of the virtual photon four-momentum. Thus we define

$$\nu = E_f - E_i,\ Q^2 = -q^2; \tag{1.1}$$

where ν is the incident particle energy loss, E_i and E_f are the energies of the same particle in the initial and final state respectively, q is the force carrier's four-momentum and Q is a conventional quantity defined in order to avoid dealing with negative squares. Now, if the scattering is elastic, energy conservation bounds one of the two parameters and the other describes completely the interaction; namely the force carrier's energy always corresponds to the loss of the probe, but it equals the kinetic energy of the target after the collision only under the condition provided by elasticity: in this case

$$\nu = \frac{Q^2}{2M}, \tag{1.2}$$

where M is the mass of the target. In the more interesting case of inelastic scattering, however, no such condition is required; therefore ν and q^2 are totally independent variables.

A leading role in this kind of process is played by the effective area of the target particle, which goes by the name of cross section σ; though, the information carried by this parameter is too approximate and the main observable of scattering experiments is usually the differential cross section. The latter is a function of the free parameters which describe the collision and measures the effective area that results in a situation characterized by those parameters. In the case of an inelastic process, for instance, it measures the imaginary surface $d\sigma$ whose hit results in a final state with an energy loss of the probe between ν and $\nu + d\nu$ and a momentum transfer between Q^2 and $Q^2 + dQ^2$.

Elastic processes, which involve lower energies and are therefore easier to set up, were examined first, and it did not take long for scientists to observe that experimental data from this source did not agree with the differential cross section formula for Dirac's point-like particles. Eventually a detailed analysis of elastic scattering led to the conclusion that nucleons had indeed a finite radius. Through the measure of the cross section it was possible to parametrize the deviation from the point-like behaviour with two functions, named form factors, which were discovered to be actually the same function and, from a physical point of view, were no other than the fourier transform of the proton charge distribution.

1.2 Incoherent interaction and scaling

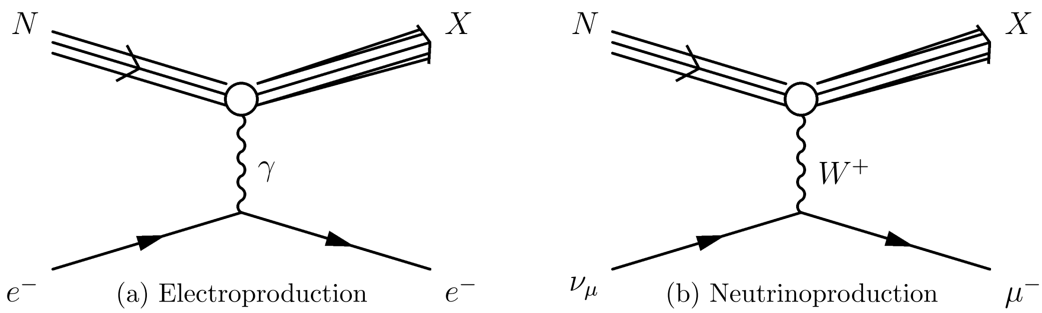

Figure 1.1: Examples of the two main classes of deep inelastic processes.

The case of deep inelastic scattering (DIS) is more complex and yet more intriguing altogether. In the picture above the Feynman diagrams for the two main classes of deep inelastic processes are shown. The first kind, named electroproduction, involves the use of a charged lepton (usually an electron or a muon) to investigate the nature of the nucleon; the most common collision mechanism is that of a single photon exchange and the whole process is mainly led by the electromagnetic interaction. In neutrinoproduction the probe is actually a neutrino, which does not have an electric charge and cannot take part in electromagnetic processes, thus making weak force the leading interaction.

The idea below these experiments is that a more energetic particle, according to Heisenberg's uncertainty principle, can resolve much smaller distances and see *deep* inside the nucleon. In order to obtain this result the energy of the probe must be high enough and, consequently, the collision often has a devastating effect on the target, causing the distruction of the latter and the formation of new particles. The process is accordingly *inelastic*.

Particle creation carries a new issue: a whole jet of objects, each with its four-momentum, needs to be handled. This problem is usually dealt with by treating the products of the disintegration as a single fictitious particle whose four-momentum P is the sum of all the four-momenta p_i of the sub-products. One straightforward consequence of this treatment is that the imaginary outgoing object has a mass that is given by the square root of the norm of its four-momentum, and is called the invariant mass W of the particle set which it stands for. Namely, we take

$$P = \sum_i p_i,\ W^2 = P^2; \tag{1.3}$$

if the target four-momentum, in a frame where the target itself is at rest, is denoted by p, the four-momentum conservation law leads then

$$P = p + q,\ W^2 = P^2 = (p+q)^2 = M^2 + 2M\nu - Q^2. \tag{1.4}$$

Another important variable is the ratio x of the energy that the target would have acquired if it had remained whole and had kept its original mass compared to the energy carried by the photon. Hence we define

$$x = \frac{Q^2}{2M\nu}, \tag{1.5}$$

and, as x equals one when energy conservation holds and zero when all the energy brought by the photon results in no momentum transfer, it measures somehow the "elasticity" of the event.

When experimental data became available, it was natural to parametrize the empirical differential cross section with structure functions, which were to play for DIS the role that had been covered by form factors in elastic scattering. Namely, it was assumed that

$$\left(\frac{d^2\sigma}{dQ^2 d\nu}\right)^{eN} = \frac{4\pi\alpha^2}{Q^4}\frac{E_f}{E_i}\frac{1}{M}\left[2F_1^E(Q^2,\nu)\sin^2\frac{\vartheta}{2} + \frac{M}{\nu}F_2^E(Q^2,\nu)\cos^2\frac{\vartheta}{2}\right], \tag{1.6}$$

$$\left(\frac{d^2\sigma}{dQ^2 d\nu}\right)^{\nu N} = \frac{G_F^2}{2\pi}\frac{E_f}{E_i}\left[2F_1^W(Q^2,\nu)\sin^2\frac{\vartheta}{2} + F_2^W(Q^2,\nu)\cos^2\frac{\vartheta}{2} \pm F_3^W(Q^2,\nu)\frac{E_i+E_f}{M}\sin^2\frac{\vartheta}{2}\right], \tag{1.7}$$

where the first equation is for electromagnetic events and the second refers to weak-interaction-led processes. The trends of F_1^E, F_2^E, F_1^W, F_2^W and F_3^W were determined by requiring the relations above to hold.

It was thus found, starting from physical experiences, that the structure functions' dependence on the variables Q^2 and ν is extremely simple (as long as the values of the two parameters involved are high enough), and that in the case of charged lepton - nucleon interaction the two functions are tightly related. As a matter of fact there were theoretical conjectures enough to expect these behaviours.

First of all it must be considered that in the case of elastic scattering the mass of the nucleon, which does not change during the interaction, naturally sets a dimensional length scale for the reaction, while in DIS there is no quantity to perform this task. Therefore it is not surprising to find that for high Q^2 and high ν the structure functions, which are pure numbers, show dependence only on the value of a dimensionless combination of the two. The variable x defined as above can be chosen to cover this position, in which case the behaviour that has just been described and goes under the name of *Bjorken scaling* can be formally stated as follows:

$$F_1(Q^2,\nu) = F_1(x),\; F_2(Q^2,\nu) = F_2(x). \tag{1.8}$$

The close relationship between the two functions was the equality that links structure functions for spin-1/2 particles, namely

$$F_2(x) = 2xF_1(x), \tag{1.9}$$

and was interpreted as a hint for the existence of fermion constituents.

1.3 The parton model

It has been argued that the lack of a dimensional quantity to set the length scale of the reaction shows up in scaling; now we want to show that this property has a more far-reaching physical interpretation, if one is to set up a model to explain the internal structure of the nucleon. The spatial extent of this particle was revealed by elastic scattering experiments which were able to produce a number for its radius: by means of the Fourier transform it was possible to find a value of about 0.8 femtometers for the radius of the sphere representing the proton charge distribution. Nevertheless the absence of a scale in DIS experiments suggests an interaction of the photon with a dimensionless, that is point-like, object. Following the path that starts from this observation, and making no other assumption, it is possible to develop a model where an undefined number of point-like particles named *partons*, carrying unspecified charge and momentum, builds up the nucleon.

A brief but important observation must be made before reaching further conclusions. Saying that the virtual boson which mediates the interaction between a lepton and a nucleon hits a single dimensionless object implies that the object itself is free on the spacetime scale of the collision, otherwise a third particle bound to the target would take part in the event too and this would show in the analysis. Namely, if the time of the electron-parton interaction were large enough to allow interparton information exchange, the struck particle would carry or push away another and the involved target would be made of two particles; another length, the mean distance of the partons, would then become important and hide the scaling feature. As experimental evidence is against this conclusion it must be assumed that, at high energies where scaling shows, the virtual boson exchange between the lepton and the struck parton is quick enough to be finished before the other partons become aware that something's happening. Thus the force that binds partons together, which goes by the name of *strong interaction*, slackens asymptotically for small distances and high energies; this feature is referred to as *asymptotic freedom*.

Let now $f_i(x)$ be the probability distribution function for the i-th parton to carry at a given time t a fraction x of the total four-momentum of the nucleon. Starting from these *parton distribution functions* (PDFs) and from the known expressions for the differential cross section of dimensionless particles, it is possible to evaluate the cross section of the nucleon both for weak and electromagnetic interaction. Comparing these relations with equations 1.6 and 1.7 it is possible to link structure functions to the probabilities f_i, and thus to gain information about the nucleon parton composition from experiments. While this comparison operation is carried out, the argument of the structure functions, which arises naturally in the computation of the cross section and actually happens to be the fraction of momentum x borne by the struck parton, is identified with the scaling variable. Therefore, under the hypoteses of the parton model, these two quantities coincide and the rudeness of using the same symbol to indicate both up to this point may be forgiven.

Using the tools built together with this model it is possible to extrapolate the contents of experimental data from structure functions to PDFs, whose interpretation is much more straightforward. Through processes mediated by the electromagnetic force one may tell apart distribution functions associated with different charges and magnetic moments, while using the information from neutrino-nucleon scattering matter and antimatter contributions to the total differential cross section can be separated. The result of this process is a set of PDFs which represent the internal structure of the nucleon, thought as an object composed of many point-like particles.

1.4 Quarks and confinement

When Feynman and Bjorken came up with this model, there was another field of research in particle physics whose results were immediately related to partons: particle classification. The huge host of different particles which had been discovered had called for a logical scheme to organize them, and the search for such a classification had been answered best by Gell-Mann's quark model. This phenomenological theory had split the known hadrons into multiplets, and counted on the possibility of seeing strongly interacting particles as composed of two or three simpler objects named quarks to classify them. By the assumption of the existance of three different kinds of quarks, or flavours, hadrons were divided into multiplets according to an $SU(3)$ symmetry scheme. The success of this hypotesis was astonishing, especially for people who did not believe in the physical reality of quarks yet. As a matter of fact many scientists thought at first that the success of these supposed constituents of the nucleon was limited to particle classification, but when the parton model was developed it reminded immediately about quarks.

Nowadays six kinds of quarks have been succesfully observed, coming up in three isospin doublets very much like leptons.

$$\begin{pmatrix} u \\ d \end{pmatrix} \begin{pmatrix} c \\ s \end{pmatrix} \begin{pmatrix} t \\ b \end{pmatrix} \tag{1.10}$$

The six quark flavours (up, down, charm, strange, top, bottom) divided in doublets

As a matter of fact, it seems that every elementary fermion comes in three versions, which can be told apart only because they have different masses. Inside a strong isospin doublet, instead, particles can be distinguished only because of the presence of the electromagnetic interaction, i.e. they differ because of their charge, and of nothing else.

According to the quark model every meson is made up of two quarks, while every baryon, including the nucleons which are the object of this research, is composed by three. Nevertheless, one must not hurry to the conclusion that these contituents alone account for all the properties of the hadrons, as the presence of other objects inside of them cannot be ruled out *a priori*; it was thus very good that in building up the parton model no assumption about the number of partons was made.

Particle classification had taught a lot about the quantum numbers (i.e. charges, isospin, baryon number...) of quarks, and it was then straightforward to use this information to determine quark PDFs for the nucleon setting as unknown a probability function for each light flavour. Through experimental determination of parton distribution functions it was thus confirmed that the momentum fraction carried by up and down quarks in neutrons and protons is in good agreement with the hypotesis of quark composition made for particle classification, and it was discovered that there seems to be a small amount of antimatter inside any matter baryon. Nevertheless, though momentum ratios determined through PDFs are in good agreement with predictions from the quark model, the contributions of the light-flavoured quarks account only for half of the total momentum of the nucleon; this has been interpreted as an evidence for an important presence of uncharged strong-force carriers inside hadrons.

Anyway, what was said leads to the conclusion that the structure of the nucleon is complex, and that the three constituent quarks suggested by the flavour symmetry scheme, sometimes called *valence quarks*, are but a part of it. Indeed, when a more detailed analyses is carried out, traces of quark-antiquark pairs from the vacuum sea (known as *sea quarks*) and strongly-interacting bosons named *gluons* may be seen.

A last phenomenological observation must be made before venturing in the speculative side of this matter. This is to do with the lack of any evidence for the existence of fractional electric charges. Even in DIS experiments, where a single parton is struck hard and gains enough energy to tear the nucleon apart, no hint for the presence of isolated quarks scattering free after the collision was ever seen: the result of such an event is rather a jet of other hadrons and, eventually, sub-products such as photons or vacuum pairs. The outcomes of the parton model are so good that rejecting it just for this, however important, missing proof seems unwise; nevertheless the gap created in the theory by such a failure in observations calls for a formal statement. Namely, to save all has been done up till now, we must admit that quarks exist only inside hadrons, perhaps because they are bound so tightly that every attempt at pulling them out of bigger particles results in the much less energetically expensive production of a quark-antiquark pair. This last feature of the strong interaction is referred to as *confinement*.

1.5 Quantum chromodynamics

Two faults emerged in the $SU(3)$ flavour scheme soon after its conception: one was the total emptiness of some multiplets which were not matched by observed particles while others were filled perfectly, another was a particle which appeared to violate openly the Pauli exclusion principle. Let us examine the latter first.

The Gell-Mann theory of quarks provides for the Δ^{++} resonance particle a quark composition (uuu): this hadron finds its natural location in the spin $3/2$ baryon multiplet as made up of three up quarks. The problem is that the wavefunction associated to the given charge and angular momentum must be totally symmetric, whilst it should be anti-symmetric under exchange of any two identical fermions such as the up-flavoured quarks are; moreover the discovery of the more exotic $\Omega^- = (sss)$ particle shows that the case is not isolated.

As a mean to escape this self-contradiction the introduction of a new quantum number, later named *colour*, was suggested: as n different eigenvalues allow the construction of a wave function totally antisymmetric for n particles, three different colours are enough to successfully perform the trick. This far-fetched hypotesis was formulated *ad hoc*, but it gained much more importance because it was directly connected to a possible solution of the other mentioned problem.

In fact, the introduction of an observable such as colour allowed a classification of hadrons in another, different, $SU(3)$ symmetry scheme regardless of any flavour distinction. The fact that no evidence of a charge such as colour had yet been discovered in the known hadrons was a hint to find out that only the combinations of quarks which gave birth to a colour singlet had a matching filled flavour multiplet. Thus it was concluded that only colourless (or, better, colour-balanced) hadrons could exist for a time long enough to allow their observation; the most simple combinations of this kind being a quark-antiquark pair and three quarks of three different colours. This statement is much more persuasive because it leads to look at quark confinement as a conclusion rather than a cause: as isolated quarks are not in a colour-singlet state they cannot be free. Because of their colour charge, they need to stay glued to something else to become neutral and are thus confined into colour-balanced hadrons. Furthermore, from this point of view the interaction among nucleons can be seen as a residual of the internal strong-force balancing: no net colour charge gives rise nevertheless to high-order effects which bind the nucleus together. This mechanism reminds very much of the Van der Waals force, which comes out of no net electric charge being generated by dipole and higher-order electric moments.

Now, the absence of a clear way to define a particular colour suggests some kind of independence of the strong interaction from the specific chosen colour coding, that is a symmetry under redefinition of strong charges. The three colours introduced so far can be seen as the fundamental representation of the colour $SU(3)$ symmetry group, and the lagrangian of the force due to this new charge may be required to be invariant under local colour-code redefinition. A new gauge field must then be set up to communicate this convention between different points, and treating such a field with quantum mechanics asks for the introduction of a new boson: the gluon. This is the mechanism which gives birth to gauge field theories, which has been successfully applied to develop quantum electrodynamics (QED) before anything was known about colour; when a new source of interaction was discovered it was sort of natural to hope that the same procedure could be applied again. Today the branch of physics that arises when the colour hypotesis becomes a gauge theory, whose name is *quantum chromodynamics* and is often shortened as QCD, has improved inasmuch as to enter the field of precision physics.

One of the most fascinating features of gauge theories is the variation of charges with the energy involved in the measure process. This can be made clear recalling that, according to the laws of quantum mechanics, particle pairs can borrow energy from the vacuum as long as they exist for a very short time. Let a point-like electric charge, for instance, be isolated in the void and probed by an electromagnetic interaction: the particle interacting with the charge can see electron-poistron pairs appear close to the charge and stay there for a little while. As these pairs emerge with no net charge but non-zero dipole momentum, they behave as small electric dipoles, orienting themselves and slightly screening the charge. The smaller the space resolution of the probe, the less the number of particle pairs it sees between itself and the charge: thus the electric charge looks greater when seen at short distances. As this behaviour affects all the sources of the considered field, it is usually preferred to think that it is not the charge that changes, but the constant setting the interaction strength itself. Thus the fine structure "constant" α increases with the energy involved in a process, because the screening effect of the vacuum space decreases.

A similar behaviour is shown by the strong interaction whose relevance changes with distance, but a radical difference between electromagnetic and colour forces becomes apparent when it comes to the trend of the strong coupling constant α_s. Indeed while a photon carries no electric charge, and its presence in the vacuum sea can be ignored when it comes to evaluating the shielding effect of charges because of the void medium, gluons, according to QCD, come in eight different-coloured versions and can actually interact amongst themselves. The contribution of gluon pairs must then be added to that of quark-antiquark pairs in order to obtain a correct insight of strong interaction's intensity variation, and such a factor has an anti-screening effect over colour charges. This process of gluon polarisation prevails over quark charge-shielding, thus giving the strong force a growing importance for greater distances. What has just been said is in good agreement with the features of asymptotic freedom and confinement which have been previously mentioned in their phenomenological aspects, and leads to consider the parameter α_s as a function of the length scale. As length quantities are directly linked to energies and then to masses through the two fundamental constants $\hbar$ and c, it is equivalent to express this dependence taking mass as a variable instead of length. In order to make the comparison between values as easy as possible, the most common convention used today is to express the value of $\alpha_s(m)$ for $m = M_Z$ where M_Z is the mass of the Z particle that has been measured with a very high precision during experiments at the LEP collider; if data is determined for different mass scales QCD provides the tools to evolve results till their matching M_Z-referred values.

It is worth to say that the variation of the strong interaction with energy, and particularly asymptotic freedom, plays a key role in quantum chromodynamics. Indeed no success in performing any exact QCD calculation has been achieved yet; the only way to make this theory a fertile ground is to use perturbative techniques in order to obtain approximations which can be compared to experimental results. This method may be applied only if a situation where chromodynamic effects are very small is found, and asymptotic freedom guarantees that short distance phenomena meet this requirement.

Let us finally relate quantum chromodynamics to a last feature internal structure of the nucleon. When higher precision experiments and larger kinematical ranges were explored it was discovered that scaling as it was described above was only an approximation. Namely the structure functions show a light dependence on Q^2, and so do parton distribution functions: as the momentum transfer increases valence quarks' PDFs tend to show that these partons carry a lesser fraction of the total momentum of the nucleon. This trend is now interpreted as follows. As long as the momentum transfer involved in the process is low, the parton distribution functions of the valence quarks indicate they bring about one third of the total momentum each, but the PDFs are already far from being delta-like in $x = 1/3$ because of Heisenberg's uncertainty principle: the quarks are confined inside the nucleus, thus Δq is consequently small and Δp cannot vanish. When Q^2 gets greater, though, the probe starts to see the details of the continuous gluon exchange between valence quarks, and the production of quark-antiquark pairs induced by the presence of these gluons. The more deeply such mechanisms are seen, the smaller is the momentum fraction which appears to be carried by the three quarks: some momentum will indeed be lent for short times to sea particles or gluon, and show as missing from valence quark distributions. Although the brief summary given here is not very accurate, this explanation should account for the change of the structure functions with Q^2, which gives rise to *scaling violations*.

Chapter 2

The NNPDF approach to global parton fits

2.1 The ideas of NNPDF

The present chapter deals with the procedure used to obtain parton distribution functions, data sets employed to achieve their estimations and the key idea that transforms a parton fit into a tool which allows for a measure of the strong coupling together with the PDFs. The first observation that should be made is that, according to what has been previously said, different experiments provide different informations about partons, thus in order to produce a detailed PDF set reproducing every feature of the nucleon structure at its best it is desirable to have as a starting point a source as wide and varied as possible. This is the reason of the need for global parton fits, whose aim is exactly to build up a single optimal set of parton distribution functions.

The framework of these complex procedures can be summarized as follows. On one side there is an ensemble of measured observables alongside their experimental uncertainties, while on the other we have a collection of aspirant parton distribution functions with a number of free parameters which describe them. Basically these parameters are varied following some strategy as to make reconstructed observables as close to the empirical informations as possible. Building up measurable quantities that can be compared with empirical results out of PDFs is a difficoult business involving perturbative QCD calculations, which can be carried out at different orders.

For the purpose of the present work we use an approach named Neural Network Parton Distribution Functions, often abbreviated as NNPDF, which contemplates the usage of redundantly parametrized neural networks as unbiased interpolants. This procedure claims to be capable of a determination of the structure of the nucleon that involves no assumption on the functional form used to represent parton distributions, and to produce a faithful estimate for the uncertainties of its results; moreover it allows for the choice of any value for the strong coupling, which is a necessary requirement to apply the chosen strategy to obtain α_s.

Giving up any hypotesis on the functional form for the PDFs raises many problems which have a nontrivial solution. Indeed the mechanism that realizes such an achievement is actually the use of a highly flexible function which can manage a good interpolation for almost any point set, regardessly of its features. For this purpose a neural network with an exceedingly high number of free parameters has been chosen, mainly because of its ability at copying trends without any preference for a specific class of functions, e.g. periodic functions or polynomials. The most relevant issue is then perhaps the necessity of avoiding a fit process that ends up following, together with the true trend hidden behind empirical results, the random fluctuations around their actual values, which are an effect of accidental errors. As the fitting of a neural network to some data is usually known as training, the situation arising when this danger comes true is referred to as overtraining. A genetic algorithm is used to search for the best values of the networks' parameters, and the mentioned problem is solved by employing a specific stopping criterion for the interpolation named cross-validation; the latter prescribes to split the esperimental data available in two sets and the usage of one for the fit while the other checks the absence of overtraining. Namely at each step of the fitting process a group of random modifications for the parameters of the neural network is suggested, observables for all considered experiments are computed according to every new PDF set and the best move is chosen according to the principle of maximum likelihood, considering only the training set. This conotinuous loop is stopped either when the agreement between forecasts for validation set observables from the PDFs start getting worse, as this means that accidental errors are being fitted, or when a certain number of steps have been made, because it is likely that the fit has already converged and discrepancies with the validation points are too small to be seen.

A second chief problem that NNPDF solves with a remarkably ingenious strategy is the matter of finding a reliable value for the uncertainties affecting the PDF set. Every available datum used by NNPDF is somewhat more than a single experimental point, value and uncertainty, as it comes from many measurements: we can imagine that, to some degree of accuracy, the whole statistical distribution generated by the experiment is given altogether. Evoluting these probabilities into contours that stand for confidence level regions around the PDFs is definitely not an easy task, especially when ascertained that the price paid to obtain unbiased results includes a non-deterministic nature of the interpolation's outcome. Considered that furthermore the PDF set is influenced by theoretical assumptions and starts from a set of experiments that is not wholly self-consistent one may get an idea of the awkwardness of the issue. As a direct propagation of uncertainties from empirical probability density functions is extremely complicated, a different approach to obtain faithful confidence level contours for the PDFs is needed.

Such a strategy is given by seeing data as probability distribution functions according to the view expressed before: this way it is possible to virtually carry out the experiments an arbitrary number of times. The information on uncertainties is so transferred from a certain probability function $p(x_1, ..., x_n)$ of obtaining the observable vector $(x_1, ..., x_n)$ to a population of vectors which reproduce the original information as accurately as desired. This mechanism makes creating Monte Carlo copies of the original data set a useful tool: it allows a large-at-will number of parton set computations, whose many resulting PDFs can be later analized to obtain errors using standard statistical techniques. The variance of the functions obtained according to this method accounts then for both the experimental errors and uncertainties due to imperfect fitting.

A detailed analysis of how these concepts were developed, implemented and tested goes beyond the purpose of this work and may be found in references [2] and [1]. Here, however, it is important to underline that the strong coupling constant plays a twofold role in this analysis. First, α_s is used to evaluate the mean expected values of observables starting from the parton distribution function set through perturbative QCD techniques. A second step requiring its estimation is the calculation of kernels which allow to evolve PDFs until the scale of the considered experiment is reached. Provided that in both these points a specific entry for the strong coupling is assumed, it is possible to obtain the internal structure of the nucleon for an arbitrary value of α_s.

2.2 NNPDF versions and data sets

The analysis made by NNPDF is fully performed at next-to-leading order (NLO) in QCD perturbation theory and contemplates a basis of five to seven functions for the PDF set (depending on program release), parametrized by the same number of neural networks with more than one hundred free parameters each. The actual number of degrees of freedom is much lower, as so many variables are used to avoid interpolation bias but a much smaller set is indeed required to reproduce the functions' behaviour correctly. Anyway the ensembles of experimental points used in the present work have at least 2800 measured observables, thus to obtain rough estimations of the difference between the number of data and the number of free parameters the latter can be neglected.

Versions 1.X of NNPDF consider only DIS experiments as data sources. More precisely, these older fits included informations coming from:

- proton and deuteron structure functions as determined from fixed-target scattering experiments, as collected by the NMC and BCDMS collaborations plus a set from SLAC;
- collider experiments carried out by the H1 and ZEUS collaborations (including the FLH108 set);
- neutrino and antineutrino scattering data as collected by the CHORUS group.

Because of known problem of systematics of the HERA and ZEUS collections, these informations have been reorganized and recollected in the HERA-I combined dataset which has been employed in NNPDF since version 2.0 was developed.

As a matter of fact this version's improvements include a better treatment of heavy quark thresholds as well as some changes that make the parton fit faster an more reliable. The critical leap from releases 1.X to 2.X, however, has been made when other classes of experiments were considered together with DIS sources in order to obtain a more precise estimation. Namely, the new information gathered can be divided as follows:

- two series of observable measures, associated to the abbreviations DYE605 and DYE806, from Drell-Yan fixed-target experiments;

- some data sets from Tevatron involving vector-boson production, including CDF and D0 Z rapidity distributions as well as CDF W boson asymmetry;

- information from the second runs of CDF and D0, involving inclusive jet production.

The introduction of these sources has allowed a determination of distribution functions for the strange and antistrange quarks, which were fixed through constraints in the previous versions of NNPDF.

The kinematic region covered by these experimental points is sketched in figure 2.1. As displayed in the graph, adding the new experiments has allowed an expansion

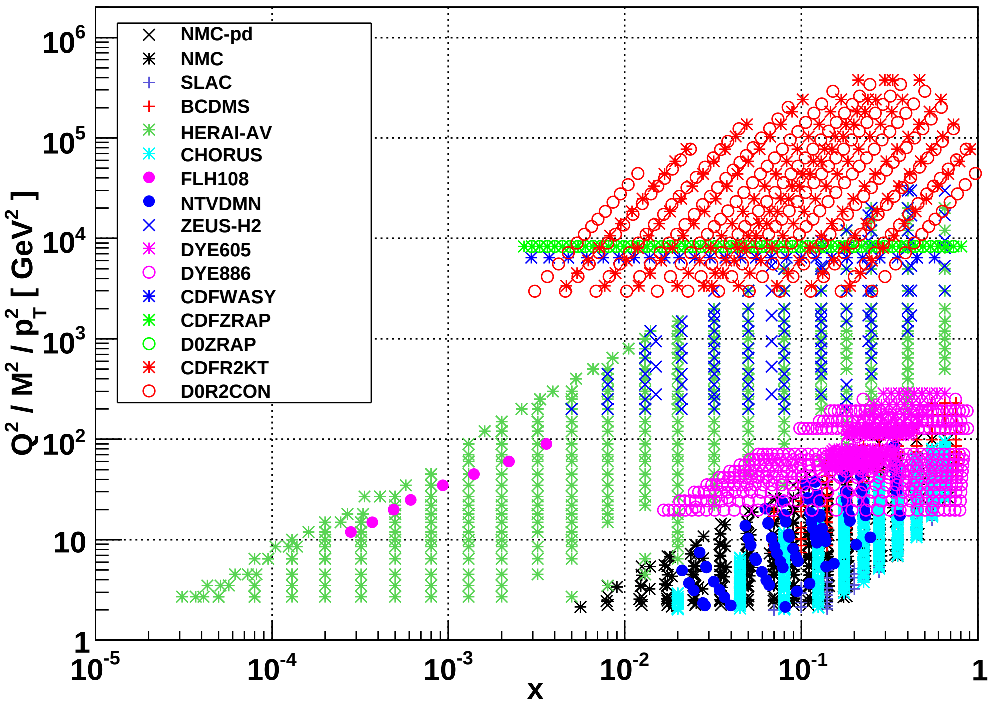

Figure 2.1: (x, Q^2) plot for NNPDF 2.0 data sets.

of the explored kinematic region towards the high-Q^2, high-x zone, together with an improvement for high-x, middle-Q^2 regions which already had some data.

Chapter 3

Statistical treatment of fluctuations

3.1 The χ^2 function and the origin of the fluctuations

Chances of improving physical knowledge are often, if not always, tightly related to the possibility of finding laws which agree with experimental data. A quantitative parameter to objectively measure discrepancies is then needed, and by accepting the principle of least squares the natural choice befalls upon the χ^2 function. If the most likely rule that fits experimental data is to be determined by decreasing the square distances of phenomenological values from law predictions as far as possible, the function which measures the sums of these squares gains a favored role. The unit to measure a square distance properly is given by the uncertainty that affects the experimental point; thus the correct expression of the χ^2 function is

$$\chi^2 = (x_i - f_i(\underline{k}))\, \Sigma_{ij}^{-1}\, (x_j - f_j(\underline{k})); \tag{3.1}$$

where Σ_{ij} is the covariance matrix for the experimental values x_i, and $f_i(\underline{k})$ is the vector of expected values for observables given the set of parameters $\underline{k}$ whose accord with empirical data is to be found.

Usually to get the best possible law which rules the trend of experimental data a class of simple enough functions is chosen, depending on one or more parameters, and the χ^2 application is then minimized upon the whole space of allowed values for those parameters. In our case the situation is only slightly different. Indeed, finding out the correct values for neural networks is not trivial as overtraining must be avoided; moreover, alongside the very high, indeed redundant, number of parameters for each parton distribution function, we have the degree of freedom provided by α_s. Thus we actually constrain one parameter, the strong coupling constant, to assume a certain value, limiting the allowed domain for variables to a submanifold of the original space, and we minimize the χ^2 inside that hypersurface. By repeating this operation for each foil of the original manifold, we would obtain a one-dimensional subset where the minimum is found for sure. As it is impossible to perform the submanifold minimization infinite times, we are satisfied by doing it for a large enough number of α_s values: assuming smoothness for the function $\chi^2(\alpha_s)$, its first derivative in the minimum point $\bar{\alpha}_s$ vanishes. It is likely (and altogether requested by theoretical arguments) to find a non-zero second derivative in the same point, thus the function, according to Taylor's theorem, should be well approximated by a parabola in some neighbourhood of $\bar{\alpha}_s$. Note that it is impossible to foretell which the said neighbourhood may be, and the answer depends on the precision required as well. Only *a posteriori* data analysis will accept or reject the hypotesis about nonvanishing second derivative and detect an interval where the parabola approximation is good enough.

Besides, by statistical arguments [5], it is possible to show that the 68% confidence interval for a single underlying parameter determined as explained above corresponds to the x-axis span determined through the condition $\Delta\chi^2 = 1$: this property shall be used to evaluate error bars for $\bar{\alpha}_s$ due to experimental uncertainties. When reading the following sections, always keep in mind that the width of the parabola which approximates the graph of $\chi^2(\alpha_s)$ around its minimum is a property of the experimental data: if no other problem affected our analysis, the parabola would provide a single exact location for the minimum point and a definite width at $\Delta\chi^2 = 1$, which could be read as the most likely value and its uncertainty according to the sources of information. The purpose of our fit for $\chi^2(\alpha_s)$, which has to deal with non-trivial complications which cloud data properties, is to recover these straightforward quantities as accurately as possible. Therefore, we would like procedure and statistical errors to be small, possibly negligible, while we want to ascertain the right value for the physical uncertainty of the result.

Stepping backwards a little, let us recall that the agreement between a certain number n of multigaussian-distributed measures and the value predicted for them by a functional form with m parameters fitted according to the principle of maximum likelihood has a probability distribution function given by

$$f_d(z) = \frac{1}{2^{d/2}\Gamma(d/2)} z^{\frac{d}{2}-1} e^{-\frac{z}{2}} \ , \quad z \in [0, +\infty); \tag{3.2}$$

for producing a certain chi square value z, where $d = n - m$. Evaluating mean and variance for this function one finds that, for a single fit, the expected value for χ^2 is given by d and its standard deviation equals $\sqrt{2d}$.

In an ideal scheme of our situation, for every Monte Carlo copy of the original data set a perfectly performed fit would result in a different χ^2 value, that corresponds to a single extraction from the probability function above. Adding replicas would allow an increasingly better sight of parton distributions and their errors, as well as an improvement in the knowledge of the χ^2 distribution function. As the mean value of a distribution is estimated with an uncertainty equal to that of the distribution itself divided by the square root of the number of extractions, the mean

χ^2 would be determined with a standard deviation of

$$\bar{\sigma} = \sqrt{\frac{2d}{N_{rep}}}; \tag{3.3}$$

where d is the number of degrees of freedom in the fit and N_{rep} is the number of replicas used.

However, the NNPDF strategy to ascertain the best interpolating PDFs is not faultless: three main error sources arise as a consequence of the adopted procedure. The first is about our data sets. Indeed, though there is no single experiment explicitly clashing with all the others, we have evidence for a certain residual internal data inconsistency of some experiments (again, see [2]). The second problem consists in theoretical hypoteses which are assumed when it comes to the determination of parton distribution functions and observable reconstruction. Positivity constraints and NLO approximations are two examples of these conjectures which may well disagree with experimental informations. The third and last element which may cause variations in the χ^2 distribution function is the imperfection of the stopping algorithm, which has been improved much in passing from release 1.2 of NNPDF to 2.0 but cannot boast to be perfect yet. If this feature is examined together with the casual nature of the genetic algorithm employed, it becomes clear that the same artificial point set can produce different replicas for parton distribution functions. Nevertheless, while the two former problems are systematics that cannot be addressed by any mean other than changing data sets and theoretical constraints, the last issue can be solved to some extent by adding replicas and averaging them.

Therefore another source of accidental uncertainty affects our chi square, making statistical error bars grow larger than $\bar{\sigma}$ and altering the shape of the probability function above. Because we believe the two effects - probability width and fit uncertainty - to be of comparable importance, we shall assume the fluctuations of χ^2 are approximately gaussian as it usually happens for uncertainties coming out of more than one contribution.

3.2 The three points method

Considered the existence of fluctuations and the functional form for $\chi^2(\alpha_s)$, the most obvious thing to do would be to fit through the available points a parabola according to the principle of least squares, i.e. looking for the one that results in the minimum χ^2. However determining uncertainties for the pairs (α_s, χ^2) resulting from replica analysis is not an easy business; thus some way to proceed without error bars is needed. Moreover the formula 3.3, though approximated, shows that for few replicas the fluctuations around the mean value of χ^2 are large. This is found to make the minimum obtained through a single interpolating parabola very unreliable. Thus, at the beginning of any analysis, finding out if everything is going as expected is a hard business.

A suggestion to develop a more stable technique has been made in reference [7], observing that some information about resulting minimum reliability is enclosed in the N_p fluctuating points (α_s, χ^2). If the chi square mean values had null uncertainty, the latter could be perfectly set on a parabola and any combination of three points would be sufficient for a perfect determination of the minimum. The central idea is then that the population of all the minima obtained through considering each subset of three points can give an estimation of how much χ^2 fluctuations can alter results. It seems that, as a greater population clearly provides better information, the choice of three as the number of elements in these subsets should be the best: two points are not enough to build a unique parabola with an unspecified vertical symmetry axis, while going for larger subsets of N_s elements would result in a smaller number of minima, as this is given by

$$N_{min} = \binom{N_p}{N_s}. \tag{3.4}$$

Let us now analize the starting situation and build up the whole procedure. Using NNPDF the whole experimental data set is copied a certain number of times and for each copy a global parton fit is carried out, later obtaining the best estimation PDF set as an average of many replicas and finally its corresponding chi square value. Note that the χ^2 map 3.1 depends explicitly on the considered data set, and so does its minimum; indeed considering only a part of the original data is mathematically translated into extracting a sub-vector and a sub-matrix, and this gives rise to a different function. Therefore, even if the program performing the global fit gives back a χ^2 value for each experiment, this is not expected to be the quantity needed to find the best-fitting parameter $\bar{\alpha}_s$ for that specific experiment. This should be clear by looking back at submanifolds: if in each foil a point is chosen by the criterion for the whole data, the resulting curve obtained does not generally include the minimum in the whole submanifold for a different function. Again, changing the chosen value for the strong coupling constant NNPDF may find suitable to worsen the agreement for a specific experiment, if one or more others make up for this worsening with a better fit. The goodness of fit obtained for each experiment is then only a measure of how well it is reproduced by the global fit and future considerations about partial chi square should be seen as purely heuristic.

Suppose now that a number of (α_s, χ^2) couples have been determined, the following steps show their analysis in detail.

(i) For each possible unordered triple of points, say

$$\left(\alpha_j, \chi_j^2\right), \ j = 1, 2, 3; \tag{3.5}$$

a parabola of the form $y = a_i x^2 + b_i x + c_i$ is interpolated by solving the linear system

$$\begin{cases} \chi_1^2 = a_i\,\alpha_1^2 + b_i\,\alpha_1 + c_i \\ \chi_2^2 = a_i\,\alpha_2^2 + b_i\,\alpha_2 + c_i \\ \chi_3^2 = a_i\,\alpha_3^2 + b_i\,\alpha_3 + c_i \end{cases} \tag{3.6}$$

in the unknowns a_i, b_i and c_i (the index i cycles on every three-points combination). The minimum is then given by

$$\bar{\alpha}_i = -\frac{b_i}{2a_i}. \tag{3.7}$$

(ii) The uncertainty range for the estimated value $\bar{\alpha}_i$ due to experimental sources is evaluated as the inverse image of the ordinate axis interval which goes from the minimum χ^2 to $\chi^2 + \Delta\chi^2$, where $\Delta\chi^2 = 1$. Accordingly we obtain the intersections between the parabola and the line $y = \bar{\chi}_i^2 + \Delta\chi^2$ by requiring

$$a_i x^2 + b_i x + c_i = \bar{\chi}_i^2 + \Delta\chi^2, \tag{3.8}$$

where

$$\bar{\chi}_i^2 = a_i \bar{\alpha}_i^2 + b_i \bar{\alpha}_i + c_i. \tag{3.9}$$

Hence, solving equation 3.8, computing the difference between the solutions and dividing by two, the parabola halfwidth that stands for empirical standard deviation is recovered

$$\sigma_i = \frac{\sqrt{b_i^2 - 4a_i\left(c_i - \bar{\chi}_i^2 - \Delta\chi^2\right)}}{2a_i}. \tag{3.10}$$

(iii) It may happen that because of strong fluctuations some of the parabolae interpolating a triple of points actually curve downwards; thus they have only a maximum instead of a minimum. We have decided that extrema of this nature should be totally ignored when using this method, because they detect a quantity which clearly does not correspond to the one we are looking for. Naturally such a choice is fully justified only when the triples discarded because of this reason are a very small ratio of the whole, otherwise the presence of many maxima suggests that fluctuations are wide enough as to make this procedure not faithful. The expected value for $\bar{\alpha}_s$ is then taken as the mean of all the actual minima α_i: said M the subset of the indexes $\{1, ..., N_{min}\}$ that stand for true minima and $|M|$ its cardinality, we have

$$\bar{\alpha}_s = \frac{\sum_{i \in M} \alpha_i}{|M|}. \tag{3.11}$$

The best estimator for the experimental error, i.e. the halfwidth of the parabola for $\Delta\chi^2 = 1$, is accordingly obtained by averaging over all the halfwidths of parabolae curving upwards

$$\bar{\sigma}_{exp} = \frac{\sum_{i \in M} \sigma_i}{|M|}. \tag{3.12}$$

(iv) Finally, it is possible to assess statistical error as the variance of all considered halfwidths:

$$\bar{\sigma}_{stat,1} = \sqrt{\frac{\sum_{i \in M} \left(\sigma_i - \bar{\sigma}_{exp}\right)^2}{|M| - 1}}. \tag{3.13}$$

The reason for such a choice, that was made in ref. [7], is heuristically that this quantity can be thought as the uncertainty upon error estimation. Nevertheless, another interesting quantity is the standard deviation of the position of the $|M|$ found minima,

$$\bar{\sigma}_{stat,2} = \sqrt{\frac{\sum_{i \in M} \left(\sigma_i - \bar{\sigma}_{exp}\right)^2}{|M| - 1}}; \tag{3.14}$$

indeed the latters reckons how much minimum position floats around its best value as all the three-points sets are scanned. Note that both these indicators vanish, as they should, when fluctuations are not considered, while $\bar{\sigma}_{exp}$ does not. Towards the end of this work, though, a motivation for another final choice to estimate statistical uncertainty will be given.

This algorithm is devised to recover in a different way the very same value and error which can be found with a single maximum-likelihood interpolated parabola; our hope is that, using such a trick, we could be able to retrieve some quantity indicating procedure uncertainty. Furthermore there is a chance that this three-points method may still be a more stable estimator for the minimum when dealing with fluctuations. Let us now look into some potential troubles that could arise during the application of the rules above.

A first weakness is somehow hinted by the *ad hoc* nature of maxima handling. In the continuous change from an upwards-oriented parabola to one that curves downwards, there is the intermidiate, degenerate case of a straight line. As soon as the function has a maximum, it is discarded, but when by some accident a triple of points is such as the parabola is nearly flat but still has a minimum, a critical situation shows up. Because of fluctuations, and because of the high number of considered combinations, this happens pretty often. The minimum for such a quadratic function may be very far from experimental points indeed, the uncertainty upon its abscissa being huge; proceeding as prescribed by the above recipe, however, a situation like this is not treated separately and might cause a great shift of the final mean value.

Because these unpleasant situation arises only as a result of very wide parabolae, one could feel the temptation of seeing them as worse estimation sources for the minimum position. As the meaning of the half-width at $\Delta\chi^2 = 1$ suggests, a possible way to lessen the importance of flat curves might be weighting the mean with half-widths as if they were experimental errors, namely

$$\bar{\alpha}'_s = \frac{\sum \frac{\alpha_i}{\sigma_i^2}}{\sum \frac{1}{\sigma_i^2}}. \tag{3.15}$$

Nevertheless this is a wrong operation, as we know that the true parabola underlying fluctuating points has a definite width, which is not due to analysis procedure but to experiments. We want to recover the true error bar, thus trying to apply standard weighted mean techniques is a mistake: that algorithm is to be used for a set of independent empirical measures, which our $|M|$ minima clearly are not as they come from a much smaller N_p[1].

This could be an unconvincing argument for a strategy that usually leads to good results, at least concerning the position of the minimum (its uncertainty, instead, must be evaluated as before to obtain reasonable values). Let us examine another problem then. While the mean χ^2 values for the α_s abscissa array are well-determined and correlated to each other, as they are linked by a parabolic law, their measured position is the sum of this specific trend plus a random contribution that changes independently from point to point, regardless of the distance between the corresponding values of α_s. Thus it happens that considering close points actually makes things worse, as their behaviour is chiefly determined by chance because fluctuations tend to be greater than the true difference of their chi squares. Weighing the many parabolae constructed for each triple of points with their supposed experimental uncertainties causes a critically bad mean, as these mistaken narrow functions are given even more importance. Nevertheless this is a source of error in the case of unweighted mean too, as the minimum distribution function has a systematic bias towards the x-axis regions where computed points are denser. Note that such a behaviour is most crucial nearby the true minimum, where the first derivative is null and χ^2 has very small variations. Luckily, these side-effects can be checked easily enough by picking up fairly separated α_s values according to the number of replicas that one is planning to compute.

Another operation that may be accomplished in order to weaken wide parabolae importance is a simple enforced cut of extrema falling outside the explored abscissa region. Yet one more time a bias problem arises, because the true results will tend have a displacement towards the center of the considered α_s interval; nevertheless a strong enough confidence for the right value to be well inside a span could make neglecting external minima a reasonable thing to do.

Our choice for handling the whole procedure best has befallen on writing a C++ class for the purpose. With a considerable help from ROOT's Object Oriented Technologies [3], a code that with few easy commands performs the operations above was developed.

3.3 Simulating the process to obtain distributions

In order to recover a faithful estimation for the uncertainties introduced by this method and to check its actual properties, the most straightforward way is to reconstruct the probability distribution functions for its results. Later, having a single

[1] For N_p high enough, say $N_p \geq 5$.

(α_s, χ^2) point set available with the maximum precision (i.e. obtained from all processed replicas), our final values for $\bar{\alpha}_s$ and its error shall be seen as one extraction from their respective distributions, which change alongside fluctuation width. Note that subsets with a smaller number of replicas compared to the total of performed fits may be considered but they are obviously less accurate.

Reconstruction of probabilities can be achieved by building up a toy program that, assuming an underlying known function, generates replicas of a point set adding pseudo-random artificial fluctuations of arbitrary width and shape to exact points; these data are later analyzed to obtain fictitious results of the methods that are to be tested. Each of these outcomes is to be interpreted as a single extraction from the distribution function for its value, which depends on the uncertainties assumed, on the initial chosen abscissa array of points and is characteristic of the applied procedure. The advantage of examining these results through Monte Carlo experiments is mainly in avoiding the slow fit of partonic functions that makes adding replicas a very long business and is pointless in order to understand efficiency rates for a method; obviously every connection with experimental data is lost in the creation of the toy program and its utility is limited to testing procedure properties.

In building up the C++ code that was to carry out this work, it has been decided that a further algorithm, intermediate with respect to the three-points method and the maximum-likelihood parabola, should be tested. More precisely, considering points in groups of four allows for a number of minima which is lesser than that of the three-points method and yet still high. On the other side interpolating four points requires a fit that is not trivially satisfied with 100% confidence level. Thus every operation made for the triples was implemented for 4-tuples to check which choice was indeed the best.

The following list goes through a more precise sketch of what the toy program actually does.

(i) Starting from a given parabola $y = ax^2 + bx + c$ and a given x-values array, the program generates through a TRandom3 object [3] an "experimental" made-up set of points, extracting them out of a probability distribution centered around the "true" value and with a chosen variance.

(ii) It interpolates one parabola through all the points, and retrieves its minimum and half-width.

(iii) It applies the three-points method, getting back the meaningful quantities for $\bar{\alpha}_s$, σ_{exp} and σ_{stat}. For this step the mean can be evaluated both weighing minima or not, and the statistical error can be chosen to be the variance of minima position or that of half-widths. Moreover, the cut discussed above can be made, neglecting minima that fall outside the considered interval when computing averages and standard deviations.

(iv) The very same operation is repeated for the four points method, the only differences being subset selection and interpolating technique. Identical options are available.

(v) The program iterates this procedure a huge number of times, building up histograms which represent results obtained through the selected methods for different amplitudes of fluctuations.

Note that the cuts of far minima are made inside each estimation for mean quantities, that is during each procedure, and not on the final histogram. The code is conceived to allow modification at will for important parameters such as the formula of the parabola, the x values for which y points are computed, uncertainties width and the number of simulations.

We have chosen a gaussian probability distribution function because of the reasons explained at the end of section 3.1. In order to make graphs and numerical results look real as much as possible (this has no consequence upon method goodness), for the analysis that follows, the parabola has been chosen to have the minimum for $\alpha_s = 0.118$ and an half-width of 0.002, as these are approximately current results for its value [8]. The minimum value of χ^2 has been set at 3415, its expected outcome for data sets without inconsistency; note that this parameter has no effect whatsoever upon the resulting distributions, as it does not affect positions of minima and widths on the x-axis.

3.4 Results

At first, a set of eleven points centered around the parabola minimum and spaced one from another as much as the parabola half-width, namely

$$\{0.108, 0.110, 0.112, 0.114, 0.116, 0.118, 0.120, 0.122, 0.124, 0.126, 0.128\},$$

has been used. Note that these values are perfectly symmetric with respect to the said minimum. The resulting histograms for the best estimates of the strong coupling according to the different methods are shown in figure 3.1, while their matching experimental uncertainties histograms can be seen in figure 3.2. For each histogram a set of 1000 simulations has been used; the resulting shapes are smooth enough to guarantee that the number of toy computations is as high as is needed for results to be stable. Each row of the graph sheets is associated to a specific variance of the fluctuations, which takes the values 5, 10, 15 and 20 when going from page top to bottom; all the histograms have the same scale and could have been drawn in the same pad, though it has been decided to divide them in order to allow an easier reading of pictures. The first column refers to results obtained through a single parabola which interpolates points best according to the maximum likelihood principle. The second and third columns are related with the four- and three-points methods respectively. In each pad for the means of these two columns three graphs are drawn: the darkest represents results obtained through weighting minima with

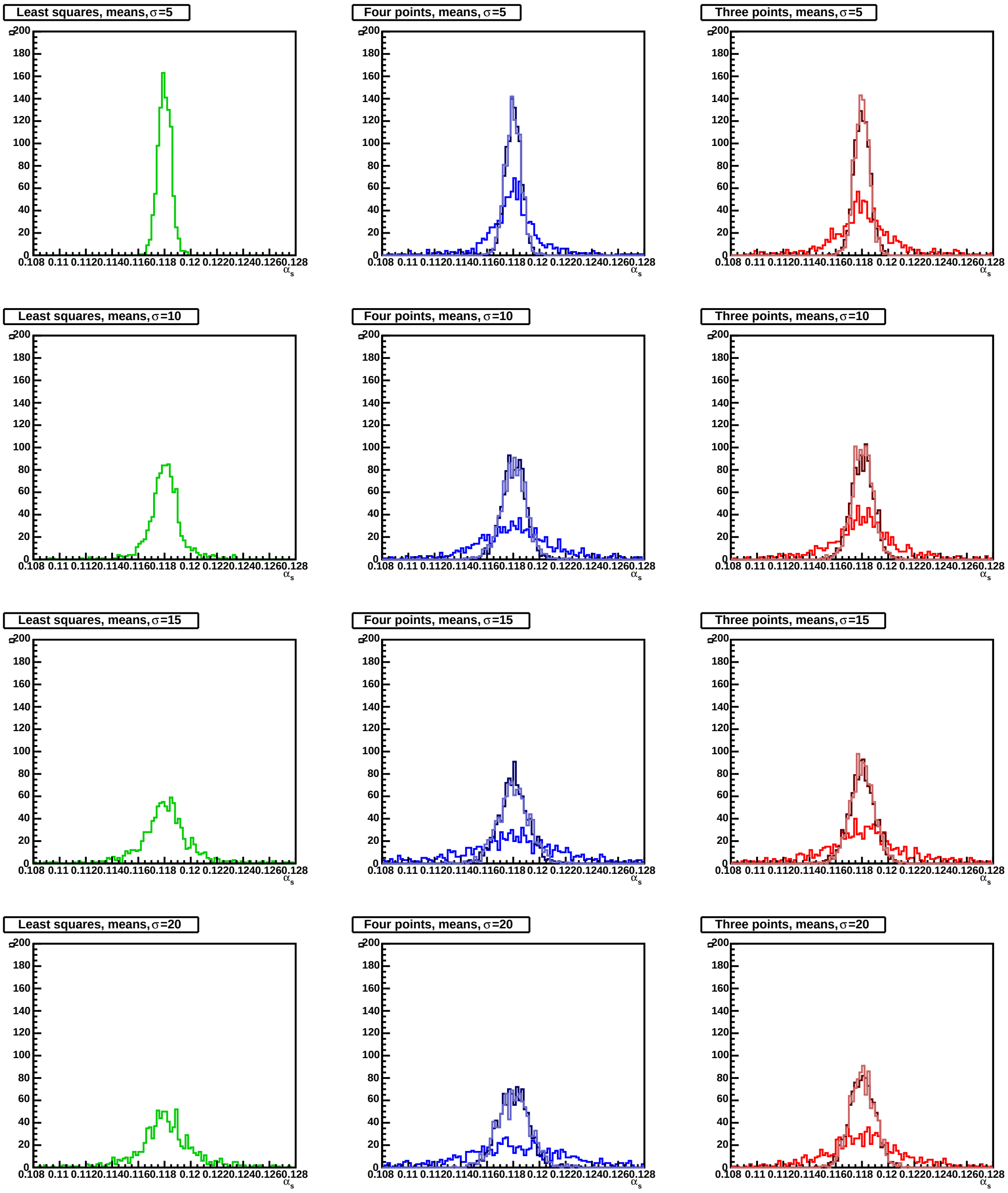

Figure 3.1: Distribution of minimum estimates for different values of fluctuations, symmetric case.

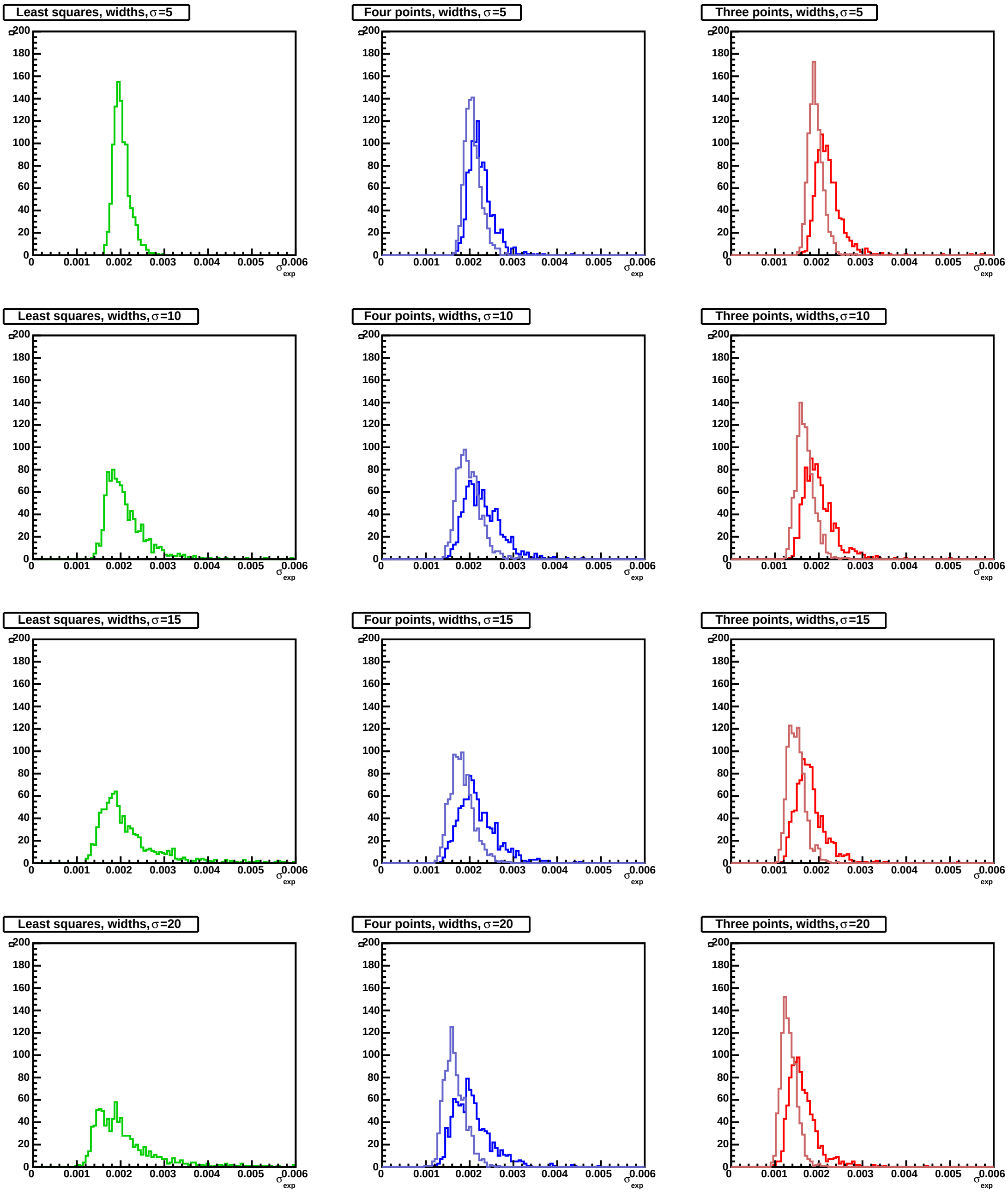

Figure 3.2: Distribution of width estimates for different values of fluctuations, symmetric case.

σ_F	All Points	Four Points			Three Points		
		uncut unweighted	uncut weighted	cut unweighted	uncut unweighted	uncut weighted	cut unweighted
5	0.1180± 0.0005	0.1180± 0.0022	0.1180± 0.0006	0.1180± 0.0006	0.1180± 0.0025	0.1180± 0.0006	0.1180± 0.0006
10	0.1180± 0.0013	0.1180± 0.0032	0.1180± 0.0009	0.1180± 0.0010	0.1180± 0.0029	0.1180± 0.0008	0.1180± 0.0009
15	0.1180± 0.0020	0.1179± 0.0035	0.1180± 0.0010	0.1180± 0.0012	0.1179± 0.0030	0.1180± 0.0009	0.1180± 0.0009
20	0.1179± 0.0025	0.1181± 0.0040	0.1180± 0.0012	0.1180± 0.0013	0.1180± 0.0033	0.1180± 0.0010	0.1180± 0.0010

Table 3.1: Values of $\bar{\alpha}_s$ best estimates and their variances, changing with fluctuations - symmetric case

σ_F	All Points	Four Points		Three Points	
		uncut	cut	uncut	cut
5	0.0020± 0.0002	0.0022± 0.0003	0.0021± 0.0002	0.0022± 0.0003	0.0019± 0.0002
10	0.0021± 0.0005	0.0023± 0.0004	0.0020± 0.0003	0.0020± 0.0004	0.0017± 0.0002
15	0.0021± 0.0006	0.0022± 0.0004	0.0018± 0.0003	0.0018± 0.0004	0.0015± 0.0002
20	0.0021± 0.0008	0.0021± 0.0004	0.0017± 0.0002	0.0017± 0.0003	0.0013± 0.0002

Table 3.2: Values of experimental error estimates and their variances, changing with fluctuations - symmetric case

parabola widths at $\Delta\chi^2 = 1$ as error bars, the middle colour stands for the method as it was originally conceived, without weight nor cuts, while histograms referring to averages with cuts (as explained above) are traced with a lighter shade. In the picture which show half-widths histograms the graphs for weighted means have not been drawn, because taking as minimum uncertainty the outcome of the weighted mean procedure leads to a sure underestimation of experimental errors, while the use of a simple mean of half-widths is already shown for the unweighted procedure. Numerical results for means and standard deviations of all drawn graphs may be seen in tables 3.1 and 3.2. Let us now look closer at mean graphs.

A general, expected behaviour is the flattening of initially peaked distributions for higher values of fluctuations; as one can see looking from top to bottom of the page, every probability function shows this trend. One more observation should be made immediately, as it is astonishingly apparent: the two histograms of uncut weighted mean and cut normal mean are very close, almost overlapping one another both for the three- and four-points methods. This is surprising but not unexpected, as the two tricks of weighing and cutting were devised to solve exactly the same trouble, that is to bypass wide parabolae. The reason of their giving rise to a more sharply peaked probability function, compared to the rather low and smooth normal mean, is quite obvious, as avoiding far minima they produce estimates which are much more concentrated.

The observation that really matters, though, is comparison with the least squares distribution. The histograms for three and four points procedures without weighted mean or cuts tend to be quite mashed compared to the green one, this means that there is no advantage in considering those methods as it would imply the extraction of $\bar{\alpha}_s$ from a wider probability function. The possibilities of finding an unreliable value thus grow larger, making these techniques useless.

A brief digression is now needed to understand observed behaviours better. It has been often said that fluctuations can be "big" or "small", but this is quite an obscure speaking as, until now, no comparison term has been set up. A quantity detecting the scale for χ^2 uncertainties must be found. The first step towards finding such a measure unit may be made by observing that, without the assumption of certain α_s values and their χ^2 computation, no specific $\Delta\chi^2$ interval would have any reason to be chosen as the scale for fluctuations. Indeed, a parabola does not have a preferred finite y-axis range. Nevertheless, we consider only a finite horizontal set, and we cannot expand it at will as, likely, far away from the minimum the trend of our function won't be parabolic. Then a possible choice for the scale parameter Δ may befall upon the explored interval of χ^2, that is

$$\Delta = \max_{i,j<N_p} \left|\chi^2\left(\alpha_i\right) - \chi^2\left(\alpha_j\right)\right|. \tag{3.16}$$

Though, as it may happen that only few points have differences so great, probably the right scale to describe fluctuations will be some kind of average of these χ^2 gaps. By the way, the order of magnitude of this parameter is all that matters and we now have an idea of its value: as vertical distances between points change from 1 to 25 for the considered parabola, we may well assume that the fluctuation scale is about 10.

For small values of the fluctuations, that is in the first line of graphs, the least-squares parabola is the best estimator for the position of the minimum, as it is the most narrow. Still, for high uncertainties, i.e. when only few replicas have been processed, the three points method, weighed or with cuts, looks sharper and should be preferred. The four points procedure seems worse than the three points method for high fluctuations: the reasoning about maximization of the number of combinations made in section 3.2 was right.

However the considered situation is a very special one, and we have arguments to believe that these trends will not hold if the reflection symmetry around the parabola axis is broken. Thus, let us consider the following point set:

$$\{0.108, 0.112, 0.114, 0.116, 0.118, 0.120, 0.123, 0.124, 0.125, 0.126, 0.128\};$$

this array's interval is again centered around the position of the minimum, but its density is no longer uniform being greater on the right side. The results for $\bar{\alpha}_s$ given by our toy program in this case are summarized in figure 3.3 and in table 3.3.

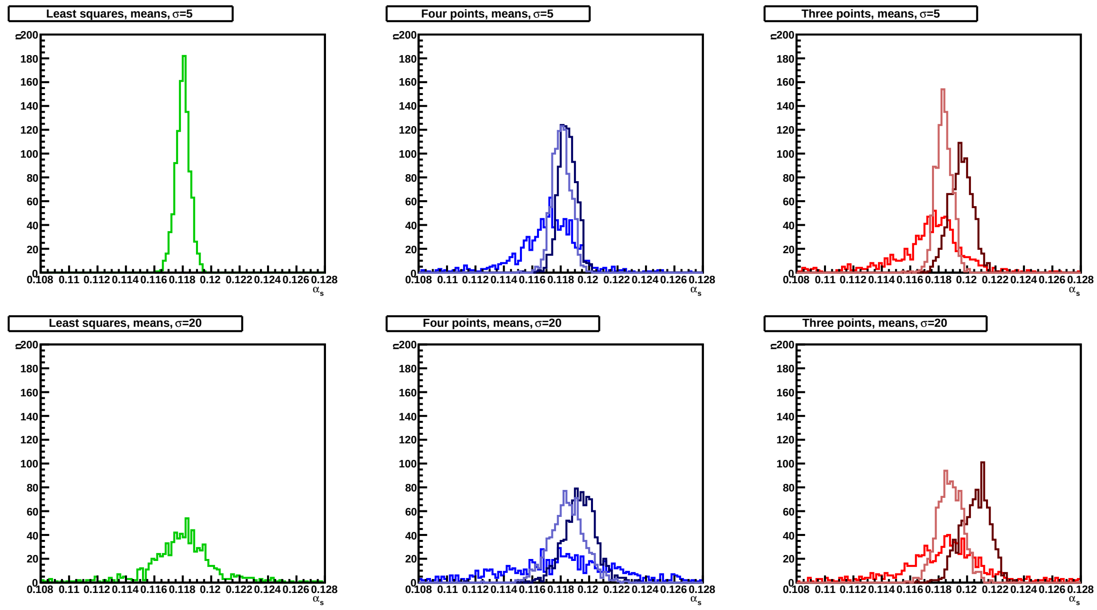

Figure 3.3: Distribution of minimum estimates for different values of fluctuations, asymmetric case.

σ_F	All Points	Four Points			Three Points		
		uncut unweighted	uncut weighted	cut unweighted	uncut unweighted	uncut weighted	cut unweighted
5	0.1180± 0.0005	0.1170± 0.0021	0.1185± 0.0006	0.1181± 0.0006	0.1175± 0.0025	0.1196± 0.0008	0.1184± 0.0006
10	0.1179± 0.0013	0.1174± 0.0033	0.1189± 0.0009	0.1183± 0.0009	0.1182± 0.0029	0.1202± 0.0009	0.1186± 0.0008
15	0.1178± 0.0022	0.1177± 0.0037	0.1192± 0.0011	0.1184± 0.0012	0.1184± 0.0031	0.1204± 0.0010	0.1187± 0.0009
20	0.1181± 0.0025	0.1182± 0.0039	0.1195± 0.0012	0.1186± 0.0013	0.1184± 0.0030	0.1206± 0.0011	0.1189± 0.0009

Table 3.3: Values of $\bar{\alpha}_s$ best estimates and their variances, changing with fluctuations - asymmetric case

In table 3.1 every mean value estimation was correct within about one standard deviation of the mean, i.e.

$$\sigma_{\bar{x}} = \frac{\sigma_x}{\sqrt{N_{toy}}}, \tag{3.17}$$

where σ_x is the standard deviation of the considered distribution and N_{toy} is the number of simulations. Now the situation is quite different, because while maximum-likelihood results may still be considered possible the others are not: dividing points in triples and 4-tuples and averaging has outcomes which are many $\sigma_{\bar{x}}$ away from the two values. Histograms clearly show a displacement of the four-points standard method on the left, this is probably due to close, only slightly different points that cause very wide parabolae. Indeed it must be remembered that altering α_s values has led to four points which are packed together in an interval of a mere 0.004. As a matter of fact the cut methods, ignoring far minima coming from these points, are affected by a slight shift on the right: this comes from a higher probability for dense, fluctuating (α_s, χ^2) sets to produce minima that are a pure statistical product of errors. More definite is the case of weighted means, where these effect is amplificated by being given even more importance, because parabolae generated by fluctuations and having a minimum are likely to be narrow.

If in case of an asymmetric array of α_s values cutting could still be a good option, the analysis of an off-centered point set, for example

$$\{0.112, 0.114, 0.116, 0.118, 0.120, 0.122, 0.124, 0.126, 0.128, 0.130, 0.132\},$$

makes things clearer. Indeed, as figure 3.4 and table 3.4 display, the shift of the weighted and cut means for such an array of points is indeed remarkable.

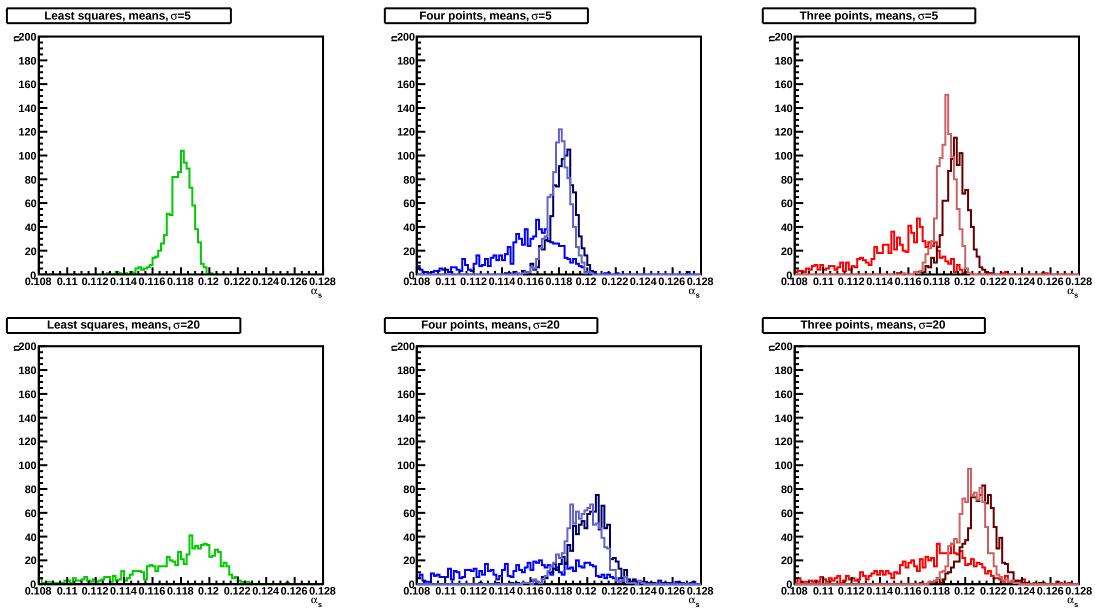

Figure 3.4: Distribution of minimum estimates for different values of fluctuations, offset case.

Note that in this case even the least squares procedure, though producing the best means, shows the symptoms of a great stress: the most frequent value does not coincide with the mean, and the probability distribution function is strongly asymmetric. An easy but nice interpretation of this behaviour may be found by minding fluctuations scales. In fact, while the average vertical distance of points on the right is huge and uncertainties upon χ^2 are consequently small when measured in appropriate units, leftwards points have small differences (the highest equals 4 in the considered case) and thus behave as if they were affected by far greater fluctuations.

σ_F	All Points	Four Points			Three Points		
		uncut unweighted	uncut weighted	cut unweighted	uncut unweighted	uncut weighted	cut unweighted
5	0.1178± 0.0010	0.1154± 0.0026	0.1183± 0.0008	0.1181± 0.0007	0.1154± 0.0027	0.1193± 0.0008	0.1187± 0.0006
10	0.1176± 0.0020	0.1151± 0.0032	0.1191± 0.0012	0.1187± 0.0010	0.1159± 0.0030	0.1203± 0.0009	0.1195± 0.0008
15	0.1176± 0.0026	0.1156± 0.0036	0.1197± 0.0013	0.1193± 0.0011	0.1168± 0.0033	0.1208± 0.0010	0.1201± 0.0009
20	0.1179± 0.0029	0.1162± 0.0037	0.1201± 0.0014	0.1197± 0.0012	0.1175± 0.0033	0.1211± 0.0010	0.1204± 0.0010

Table 3.4: Values of $\bar{\alpha}_s$ best estimates and their variances, changing with fluctuations - offset case

We may well conclude that for small fluctuations using a single interpolating parabola through all the points is by far the best method, while for high errors on χ^2 one may possibly choose to apply the three-points cut method, paying great attention to bias sources.

Concerning width distributions, evidence is against using the three (or four) points method with cuts. Cutting leads to an underestimation of the experimental error, as wide parabolae have a larger probability of yielding distant extrema, and are thus eliminated from means too often. The other distribution look faithful enough at first sight, and a naive eye may be tempted to choose the results of the three- or four-point method as their distributions are more peaked and then more likely to lead to the right result. When calculating the error upon the mean value of these probability distributions, though, one discovers that results shifted of tiny numbers from the true value are hadly compatible with it, as uncertainties are pretty small. From this point of view the half-widths coming from the second and third procedures are incorrect, yet more reliable than those of the least squares method. It is therefore appropriate to calculate both.

Chapter 4

Determination of the strong coupling constant

4.1 A new look on NNPDF 1.2 data

The first data set we will look into, now we have chosen our procedures, is the one analyzed in reference [7]. These values of $\chi^2(\alpha_s)$, summarized in table 4.1, have been obtained using version 1.2 of NNPDF, which includes as a source only deep inelastic scattering experiments.

Due to the discovery of a bug in the program which was used to study these results in the cited work, it is indeed worth to look at them again. Moreover, these data shall be a good ground for testing the discussed techniques, their strengths and their weaknesses.

Let us first consider the results obtained applying blindly to all total χ^2 points the maximum-likelihood method and the three-points cut procedure; the parabolae which are the graphical representation of means and experimental errors are drawn in figure 4.1, while numerical results are:

$$\text{Parabola through all the points: } \bar{\alpha}_s = 0.1202 \pm 0.0004(exp); \tag{4.1}$$

$$\text{Three points cut parabola: } \bar{\alpha}_s = 0.1219 \pm 0.0005(exp). \tag{4.2}$$

These outcomes do not agree with each other, and the reason for such a discrepancy is hinted by the graphs. Indeed it must be remembered that (α_s, χ^2) points resulting from NNPDF computation are not located on a parabolic curve for every horizontal interval: in this case, this may be seen by looking at the green line which should interpolate all the points, while as a matter of fact it is far too narrow to fit the left-central region and yet not bent enough to pass through rightwards data. Instead the effect on the red curve coming from these two right points, associated to $\alpha_s = 0.135$ and 0.140, is only a vertical shift: one could imagine to lower this parabola and discover that it fits the central region very well.

Another suggestion to solve the problem is the strong asymmetry of points. While for high values of α_s the graph rises steadily, it does not go up with the

α_s	0.110	0.113	0.116	0.119	0.121	0.123
NMC-pd	254.83	236.43	230.37	221.22	216.15	214.39
NMC	458.79	445.87	429.86	415.04	410.85	406.38
SLAC	152.28	134.48	122.72	117.71	118.15	124.32
BCDMS	921.49	919.20	905.39	900.63	913.88	913.51
ZEUS	569.74	573.58	549.52	543.05	539.97	540.04
H1	681.64	678.77	659.99	648.65	641.21	635.70
CHORUS	1359.41	1340.33	1306.50	1285.60	1265.64	1265.12
FLH108	14.52	14.33	13.79	13.37	12.99	12.72
NTVDMN	52.49	52.37	51.08	51.22	53.66	54.33
XF3GZ	12.44	12.25	12.25	12.30	12.36	12.55
ZEUS-H2	183.19	187.42	187.17	192.96	198.83	205.73
TOTAL	4660.82	4595.03	4468.64	4401.75	4383.69	4384.79

α_s	0.125	0.128	0.130	0.135	0.140	N_{dat}
NMC-pd	199.76	190.03	175.02	235.33	272.28	153
NMC	401.20	391.44	387.89	397.32	426.65	245
SLAC	131.99	138.85	133.88	141.08	173.16	93
BCDMS	921.43	974.65	1035.47	1335.34	1605.13	581
ZEUS	547.65	559.88	567.80	633.07	818.80	507
H1	640.16	644.19	667.91	793.74	1187.57	632
CHORUS	1262.73	1252.54	1261.37	1450.66	1735.84	942
FLH108	12.54	12.24	12.36	13.20	14.58	8
NTVDMN	55.68	59.55	61.10	88.62	117.98	84
XF3GZ	12.72	13.26	13.68	15.40	18.61	8
ZEUS-H2	214.78	233.35	246.46	295.11	368.06	127
TOTAL	4400.64	4469.98	4562.94	5398.87	6738.66	3380

Table 4.1: $\chi^2(\alpha_s)$ for experiment, data set of reference [7] obtained with 500 replicas from NNPDF 1.2

same speed on the left where it does grow less than expected from the middle-α_s region trend. All these elements whisper something about parabolic assumption boundaries: it looks like the explored interval exceeds that region where Taylor's theorem guarantees an approximate second degree polynomial behaviour. Figure 4.2 displays what happens when a third and fourth degree functions are fitted to the point set.

Even if a better fit is trivially expected when a degree of freedom is added, data agreement still gains a remarkable boost when passing from a parabola to a cubic function, while the obvious improvement in changing the interpolant to a quartic is not so critical. All this considerations suggest that the asymmetry of points with respect to the vertical axis passing through the minimum is the main source of inconsistency with the parabolic trend hypotesis.

An interesting question is how much procedural error can be blamed for this discrepancies. Equation 3.3 gives an inferior limit to the uncertainty bar that we can associate with our points, and results in a value of about 4 for this situation. Even if we assumed for true fluctuations a width ten times this size, which is a

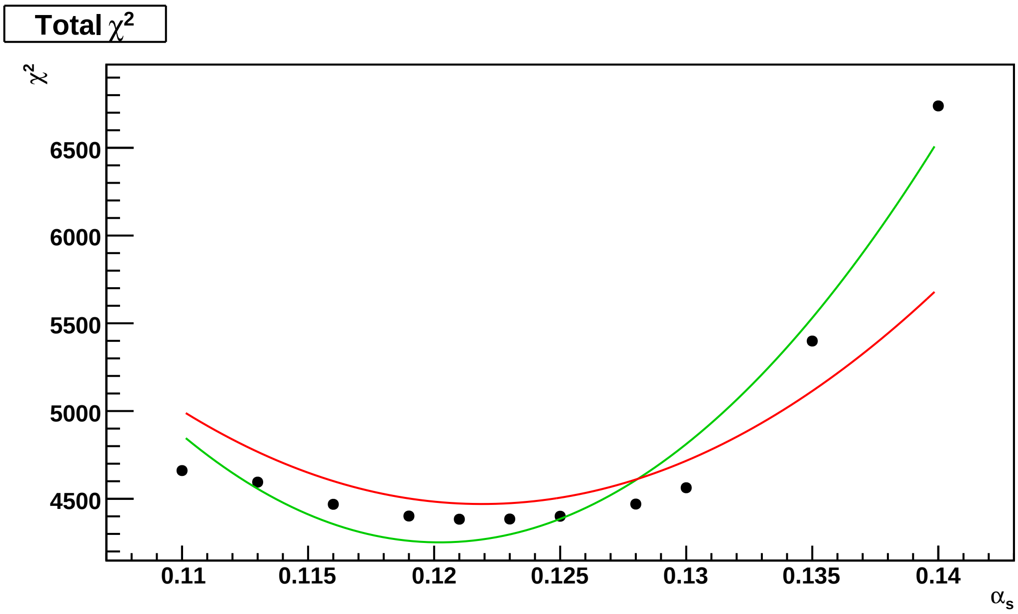

Figure 4.1: Graphical representation of results for the NNPDF1.2 data set. Green stands for least squares parabola, while in red results of the three points cut method are drawn.

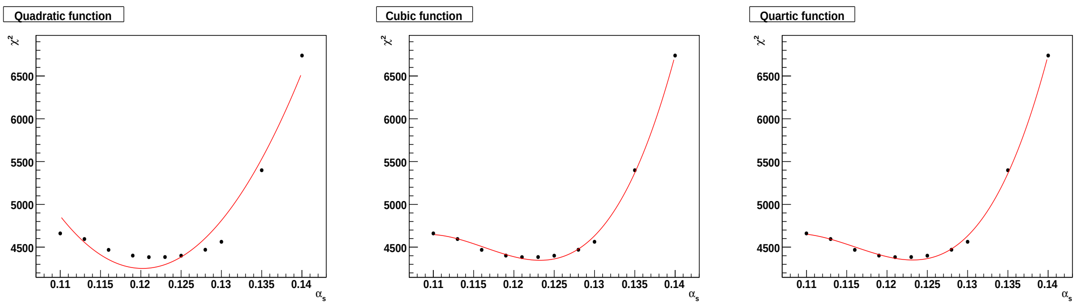

Figure 4.2: NNPDF1.2 data set fit with a second, third and fourth degree polynomials.

good deal larger than expected, still errors would be very small when drawn on the graph and would not quantitatively explain the general disagreement that appears qualitatively evident. Thus the badness of fit cannot be an effect of fluctuations and the validity of the parabolic approximation on the whole interval has been rejected by experimental evidence.

A reasonable choice to restore the conditions needed to apply our techniques is to neglect points which are further away from the minimum than, say, $20\sigma_{exp}$; as the three points method is supposed to be more similar to the next result, its values for the mean and the half-width are assumed to perform this operation. Then the x axis values not to be kept are those falling outside $[0.1119, 0.1319]$, namely one on

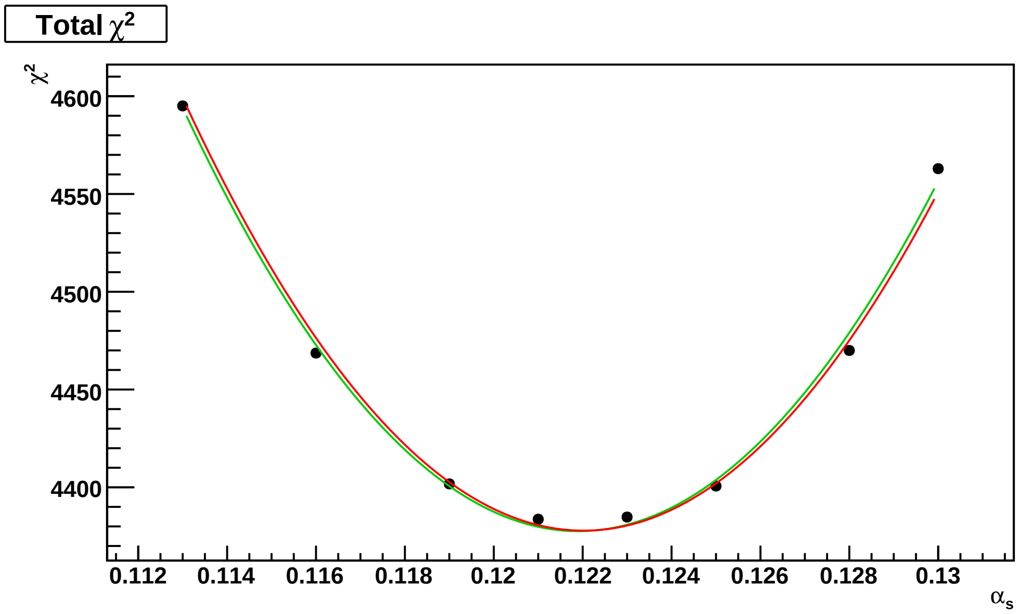

Figure 4.3: Graphical representation of results for the NNPDF1.2 data set with cuts. Green stands for least squares parabola, while in red results of the three points cut method are drawn.

the left, for $\alpha_s = 0.110$, and two on the right, which have $\alpha_s = 0.135$ and $\alpha_s = 0.140$. Note that computing the χ^2 function for the points that have just been discarded was not pointless: first, because when these results were originally achieved a firm attestation of the sensitivity of χ^2 to changes in the α_s assumption was still needed; second, because we now have an idea of how large is the interval where the hypotesis on parabolic behaviour holds.

Repeating procedures with these changes leads to the situation illustrated in figure 4.3, which numerically gives as expected values the following:

$$\text{Parabola through all the points: } \bar{\alpha}_s = 0.1219 \pm 0.0006(exp); \tag{4.3}$$

$$\text{Three points cut parabola: } \bar{\alpha}_s = 0.1220 \pm 0.0006(exp). \tag{4.4}$$

Our belief in the results obtained through the three points strategy was solid-grounded, as the outcomes of this procedure have changed very little from their former values; the interpolating parabola results have instead changed quite much, getting closer to the minimum and width expected on the basis of previous considerations. However, as we know that the maximum likelihood strategy yields better results for small uncertainties, we shall take for the best estimate of α_s its outcome. Graphs are now almost overlapping, and are in good agreement with points within an uncertainty not far from its expected value of 4; such a feature confirms that the two functions indeed measure the same object and corroborates confidence in results 4.3 and 4.4. Mind that as some points with very different values of α_s and

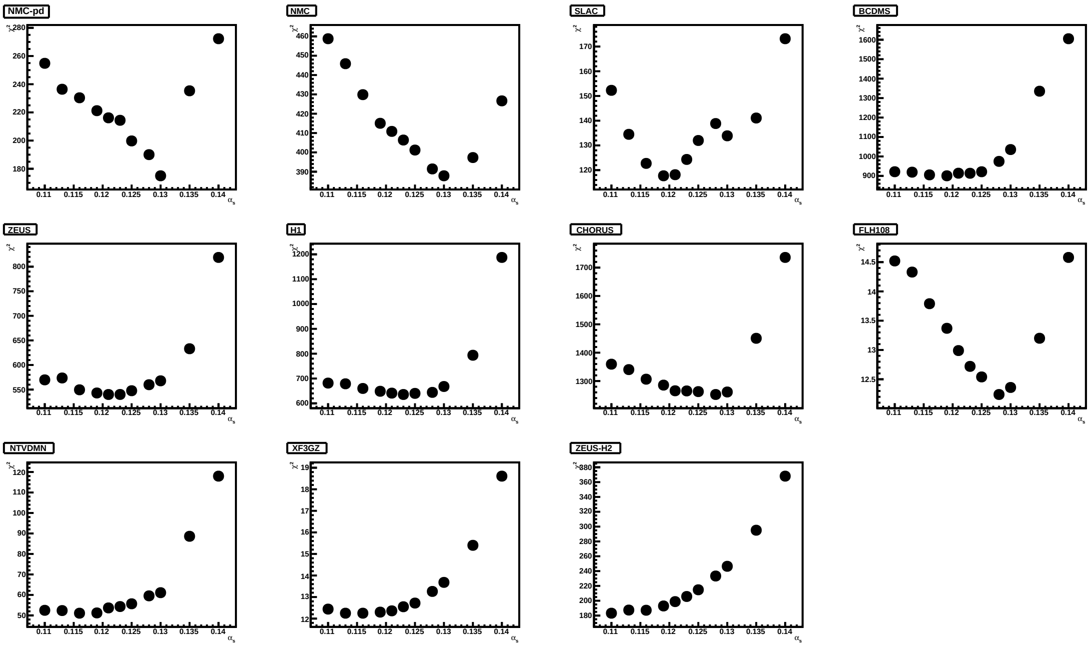

Figure 4.4: $\chi^2(\alpha_s)$ for experiments of the NNPDF1.2 data set, with respect to best estimate PDFs of a global fit.

χ^2 have been removed, the scales of both the x and y axes have changed from the previous picture.

It's worth making one last further observation about goodness of fit for the single experiments as a function of α_s, not least because results for the NNPDF1.2 χ^2 data set will be a very interesting benchmark in the analysis of more recent results. The following graphs display partial chi squares measuring the accord of each experiment with the parton distribution functions determined through global fitting. These trends lead to think that the inferior limit for the value of the strong coupling comes out of an increase in the chi square which is mainly due to NMC-pd, NMC, SLAC and CHORUS experiments. The others (with the exception of FLH108, whose χ^2 grows on the left but is quite small) look like they are actually well-fitted even for very small α_s. It seems that for weak intensities of the strong coupling some experiments, the ones which are well-fitted, lead to some PDF set which is not consistent with observables of those listed above.

4.2 A DIS-only parton fit with NNPDF2.0

As the new features we have worked upon radically change the global view given in the last section, it is most important to add them in two steps. The present section shall focus on changes in results which are due to improvements both in the program and in the organization of data sets, while the next will deal with the introduction of Drell-Yan and hadronic jet experiments as new sources of information to allow a better extraction of parton distribution functions. The main differences between 1.2 and 2.0 data are traced in section 2.2; here we concentrate upon finding the best value of α_s for the considered ensemble.

The original idea was to use a set of seven values for α_s, approximately centered on the value that is usually assumed for it and spaced as much as its uncertainty, namely $0.112, 0.114, 0.116, 0.118, 0.120, 0.122, 0.124$. Note that selecting closer values would mean to handle smaller χ^2 differences which require a higher number of replicas to carry reliable information. Moreover it must be remembered that, while the machine-time required to perform parton fits grows linearly with N_{rep}, the order of magnitude of random fluctuations around the correct χ^2 value gets lower only as $1/\sqrt{N_{rep}}$. Thus, globally, increasing the points' accuracy needs a time that increases asymptotically as the square root of accuracy itself. One could be then tempted to work with many, highly fluctuating points for very close values of α_s, but here two complications arise. First, this choice would mean dealing with hardly inconsistent data, and saying goodbye to the possibility of seeing reasonable, easily interpreted graphs. The second and more immediately compelling trouble is that for every value of the strong coupling different evolution kernels must be computed, and this requires running another program. A constant time must then be added to the length of training for N_{rep} PDF sets, if one wants to obtain the actual time needed to have N_{rep} replicas for a given point.

This is why we thought evaluating $\chi^2(\alpha_s)$ for about ten points was a reasonable decision. Then we started with the values above, plus the extra point $\alpha_s = 0.119$ whose evolution tables were already available. However, when the stage of the first 100 replicas was completed, it was difficoult to exclude the possibility of the minimum being outside the chosen interval. The fluctuations were indeed still very high. Thus it was decided to add two more points, at 0.105 and 0.130, that could work as boudaries.

Furthermore, while proceeding with the analysis, it became clear that the prediction for α_s was much smaller than expected at the beginning. Such a small value demanded for more points on the left side of our initial array, and we added one more point to extend the first set on the left as naturally as possible. We added replicas to those points until we reached the number of 500 for each (α_s, χ^2) pair and results looked stable enough. It's important to point out that, while our final results are approximately the same whichever procedure is chosen for the analysis as uncertainties due to fluctuations are rather small, in early stages the possibility of obtaining faithful estimations for the minimum abscissa has had a great influence on our choices. This is why so much attention was given to this problem in the previous chapter.

Coming back to the outcomes of the parton fit, the final numerical values of χ^2 are summarized in table 4.2.

The graph displaying the total chi square as a function of the strong coupling is shown in figure 4.5, and the best estimates for the extremum position and parabola

α_s	0.105	0.110	0.112	0.114	0.116	0.118
NMC-pd	137.05	134.52	135.23	132.71	132.32	132.30
NMC	417.73	412.73	412.58	412.86	410.59	414.05
SLAC	167.17	150.80	145.05	137.92	132.61	128.56
BCDMS	715.37	717.28	713.59	720.42	724.58	730.51
HERAI-AV	660.29	654.45	653.66	656.24	657.34	667.05
CHORUS	1044.57	1037.26	1040.64	1038.87	1039.78	1047.80
FLH108	13.77	13.03	12.76	12.54	12.32	12.24
NTVDMN	63.43	59.89	60.25	60.06	60.30	59.62
ZEUS-H2	151.45	151.03	151.75	152.05	153.79	155.79
TOTAL	3370.83	3330.99	3325.51	3323.67	3323.63	3347.92

α_s	0.119	0.120	0.122	0.124	0.130	N_{dat}
NMC-pd	131.42	131.55	131.48	132.01	131.56	153
NMC	412.62	413.28	416.16	416.03	416.77	245
SLAC	126.49	127.82	129.09	133.20	150.74	93
BCDMS	736.38	741.08	758.31	775.00	852.57	581
HERAI-AV	666.59	666.39	675.18	686.55	736.69	608
CHORUS	1054.72	1050.70	1062.50	1083.04	1113.45	942
FLH108	12.09	11.95	11.89	11.79	11.27	8
NTVDMN	60.60	60.43	60.31	60.89	61.33	84
ZEUS-H2	156.81	158.14	161.77	165.49	184.73	127
TOTAL	3357.72	3361.34	3406.69	3464.00	3659.11	2841

Table 4.2: $\chi^2(\alpha_s)$ for experiment, data set for 500 replicas, obtained with NNPDF 2.0 considering only DIS experiments

half-width determined by the application of the previously discussed methods are

$$\text{Parabola through all the points: } \bar{\alpha}_s = 0.1127 \pm 0.0009(exp); \quad (4.5)$$

$$\text{Three points cut parabola: } \bar{\alpha}_s = 0.1135 \pm 0.0010(exp). \quad (4.6)$$

It would be dishonest not to note immediately that the position of the minimum is clearly very different from the one deduced with NNPDF 1.2; nevertheless let us take this problem one step at a time.

First, it must be said that in passing from a data set of 3380 points to one of 2841, the total χ^2 has gone down accordingly. The transition from having a minimum at approximately 4380 to a best-fit chi square of 3320, however, is not wholly accounted for by the mere fall of the number of degrees of freedom; indeed (neglecting the number of parameters used from the fit, which could as a matter of fact only make our observation stronger) the normalized minimum χ^2 equals about 1.30 for NNPDF 1.2 and 1.17 for the new version of the program and data organization. This suggests that indeed the revision of experiments and of the fitting technique has solved some of the problems which are a cause of systematic errors in our analysis.

Yet the qualitative trend of points in this case is not as defined as it was in the previous section. The fluctuations around the true values of the points have actually

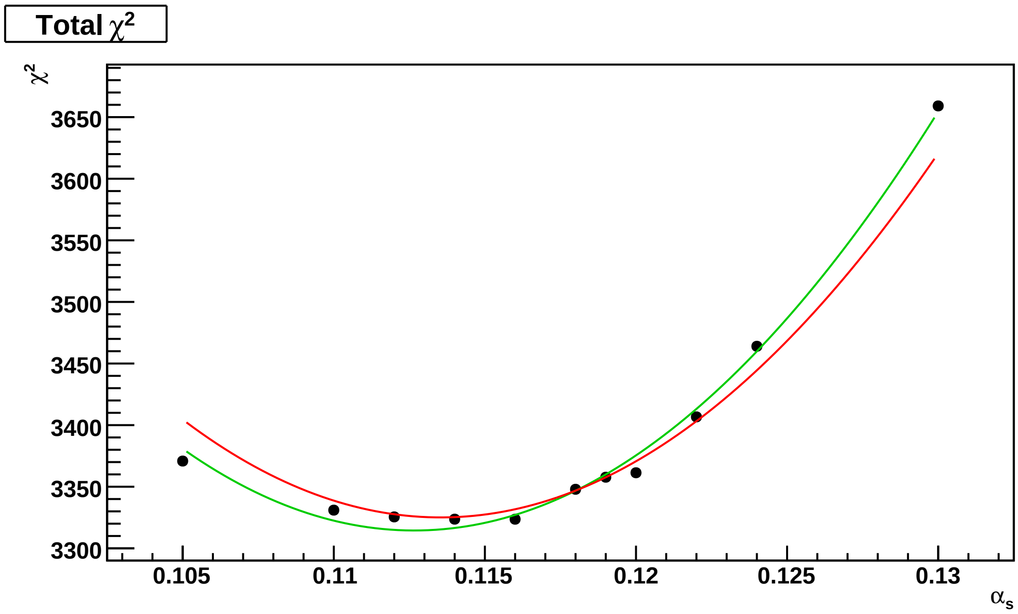

Figure 4.5: Total χ^2 for DIS experiments from NNPDF2.0.
The green parabola is interpolated according to the maximum likelihood principle, while the outcome of the three points cut method is red-coloured.

decreased a little, because N_{dat} and the average χ^2 have dropped. Though, the width of the parabola has increased a lot: removing discrepancies has led to a growth in experimental uncertainties. Furthermore the x axis span is now more narrow than before, and all of this makes the average vertical distance between points decrease. Indeed fluctuations are "big" or "small" only when referred to a scale, which this time has a much smaller unit. Giving our points an uncertainty of 3.4 as given by eq. 3.3 would already show in the picture, and we have reason to believe that this is a very rough underestimation. These reasons suggest that it is wise in the considered situation to take as final results the outcomes of the three-points method rather than those given by a single least-squares parabola, because we know the former procedure to be more reliable for high fluctuations.

To make a comparison with the 1.2 situation, within the very large value of ten times this error we would have a perfect agreement for points in the central region, and the even the most outwards points would not be incompatible with the fitting curves. Cutting extremes here would not lead to any improvement in results (and would indeed change them little), and it would not be fully justified as all considered points are closer to the minimum than the chosen quantity of $20\sigma_{exp}$.

The graphs illustrating how good is the fit for each experiment are shown in figure 4.6. As expected, there is no experiment whose accord with the model changes its behaviour completely: some get more uneven, some have slight variations. But, when looking at these picture, one must be aware of the differences in their scales, otherwise they may be misleading. Once one accurate glance has been given, it

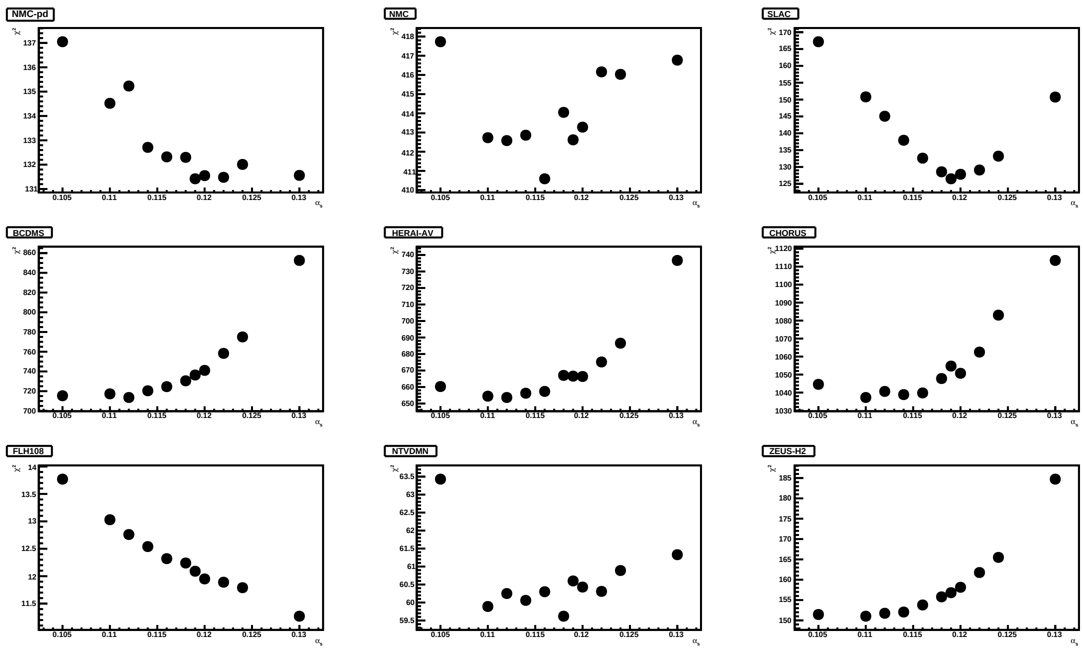

Figure 4.6: Goodness of the global, DIS limited fit for each experiment, using NNPDF2.0

looks like the reason for the great shift in the α_s value is mainly due to the absence in the new trends of the slight slope rising towards the left of the HERAI-AV and CHORUS experiments: they have a high y-axis unit and in the new graph there is no rising of theirs on the small coupling side. This could be due to the fact that, without some information pulling parton distribution functions to another value, these experiments can still be fitted very well for small α_s even in the global context. However, remember that these considerations have an importance which is not epistemological but only heuristic: to assert that HERAI and CHORUS actually prefer a certain value of the strong coupling would require to fit them separately and not as parts of a wider set.

4.3 Results including Drell-Yan, vector boson and jet experiments

We will last consider the most interesting results, coming from one of the largest available data sets which includes deep inelastic scattering, Drell-Yan, vector boson and jet experiments. Even if a close look on how NNPDF works is not included in these notes, let us point out that in passing from DIS-only to truly global parton fits the CPU-time needed to perform a fit increases dramatically from an average of 3-4 hours per replica up to 16-20 hours. The computation of a number of replicas close to 500 is required if one wants to make sure that fluctuations can indeed be neglected. Last section was aimed at highlighting differences from the different versions of the program and we decided not to refine data even if uncertainties were indeed still rather high; now we want to make an accurate measure, thus we cannot afford fluctuations to weigh on results so much.

As usual, equation 3.3 gives the minimum, ideal error on our points which, in passing from say 100 to 500 replicas it changes from about 8 to less than 4. As the mean of our χ^2 vertical distances is approximately equal to 50 (and is far lower in the central region), a number of 500 replicas is indeed needed to obtain accurate estimations. However long, this job has been fulfilled and its results are summarized below.

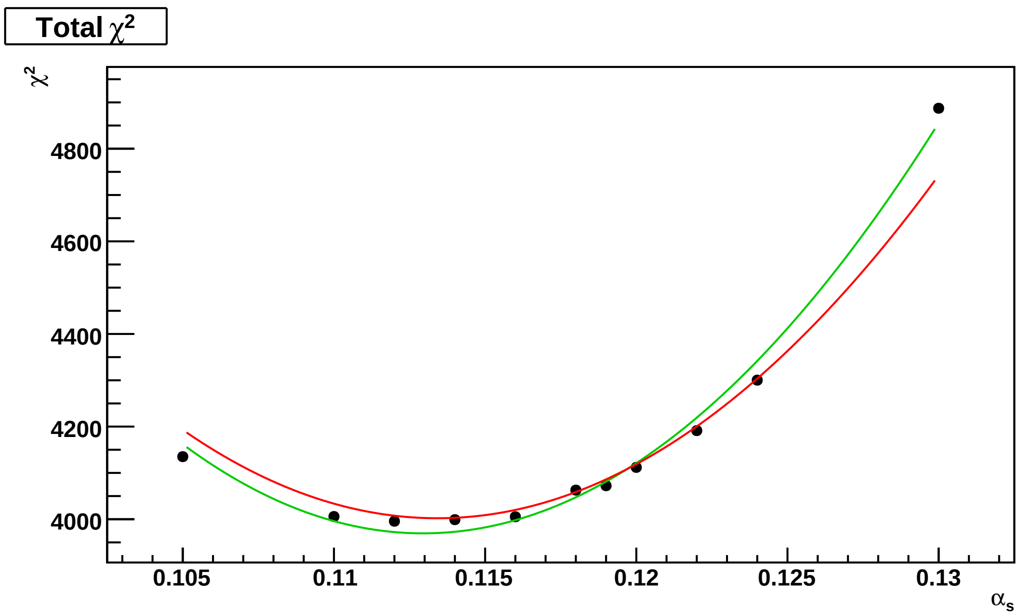

Figure 4.7: $\chi^2(\alpha_s)$ for NNPDF 2.0.
Green stands for least squares parabola, while in red results of the three points cut method are drawn.

A graphical representation of this outcomes is given in figure 4.7, and quantitatively we have:

$$\text{Parabola through all the points: } \bar{\alpha}_s = 0.1129 \pm 0.0006(exp); \tag{4.7}$$

$$\text{Three points cut parabola: } \bar{\alpha}_s = 0.1134 \pm 0.0006(exp). \tag{4.8}$$

Again the red parabola, obtained with the three points method, interpolates the central points better than the one obtained applying the least squares principle. The latter is slightly narrower because it tries to account for the last point on the right, at the expense of losing the rather flat behaviour of the point set in the middle. This effect is not as apparent as it was in the case of NNPDF 1.2, and one could be content with the results obtained. However such a phenomenon has

α_s	0.105	0.110	0.112	0.114	0.116	0.118
NMC-pd	166.69	160.87	159.18	157.60	152.85	154.24
NMC	424.76	411.26	411.23	410.86	410.03	413.66
SLAC	203.29	161.96	151.03	136.29	129.45	123.49
BCDMS	764.40	741.73	736.23	736.34	736.11	744.56
HERAI-AV	732.76	705.44	697.77	691.43	689.98	688.01
CHORUS	1090.88	1079.91	1088.05	1095.01	1093.58	1113.16
FLH108	13.54	12.87	12.70	12.51	12.35	12.11
NTVDMN	54.68	55.08	54.44	53.97	54.88	55.37
ZEUS-H2	155.95	153.65	153.04	153.92	154.44	156.37
DYE605	78.69	84.63	88.76	93.56	97.78	101.64
DYE886	197.23	209.98	214.35	227.46	234.77	248.00
CDFWASY	24.29	24.21	24.35	23.74	23.74	23.45
CDFZRAP	45.47	45.55	46.97	47.95	50.58	55.99
D0ZRAP	16.59	15.74	15.45	15.40	15.38	15.68
CDFR2KT	86.12	62.62	58.51	55.95	57.07	58.44
D0R2CON	79.75	80.35	83.65	87.07	92.35	98.64
TOTAL	4135.09	4005.85	3995.71	3999.06	4005.34	4062.81

	0.119	0.120	0.122	0.124	0.130	N_{dat}
NMC-pd	152.82	152.39	151.92	149.76	149.09	153
NMC	415.55	414.99	422.57	427.89	447.53	245
SLAC	123.62	124.06	130.18	142.21	209.86	93
BCDMS	747.82	750.03	763.06	783.60	887.01	581
HERAI-AV	683.48	683.46	684.83	687.28	775.77	608
CHORUS	1118.53	1124.20	1138.47	1154.88	1245.82	942
FLH108	12.04	11.90	11.80	11.68	11.74	8
NTVDMN	55.48	55.41	55.82	56.79	59.39	84
ZEUS-H2	157.89	158.61	161.51	165.81	186.07	127
DYE605	102.65	106.56	110.20	116.24	131.71	119
DYE886	248.44	260.30	273.68	293.00	363.35	199
CDFWASY	24.08	23.47	23.64	23.41	22.30	13
CDFZRAP	54.84	61.59	67.84	77.43	112.28	29
D0ZRAP	15.53	16.05	16.62	17.52	21.29	28
CDFR2KT	58.72	63.04	66.70	72.43	106.68	76
D0R2CON	100.86	105.86	112.52	120.33	157.42	110
TOTAL	4072.35	4111.92	4191.36	4300.26	4887.31	3415

Table 4.3: $\chi^2(\alpha_s)$ for experiment, results for 500 replicas obtained with NNPDF 2.0 including DY, JET and DIS data

been previously met, and by the simple rejection of far points a great improvement in outcome consistency has been obtained; there is then no reason whatsoever not to treat this situation as the former, even if the prompts for doing so are not as compelling as in the previous case. Now the chosen interval centered on the minimum and spanning $20\sigma_{exp}$ on both sides is $[0.1014, 0.1254]$, according to the three points method, thus only one point, associated to $\alpha_s = 0.130$, must be excluded from calculations. Such an interval selection is very approximate, and in principle it depends on the accuracy within which the parabolic approximation is required to hold. Here, as the requested precision is of the same order as before, we shall stick to the previously set convention.

By performing calculations again we obtain

$$\text{Parabola through all the points: } \bar{\alpha}_s = 0.1128 \pm 0.0006(exp); \tag{4.9}$$

$$\text{Three points cut parabola: } \bar{\alpha}_s = 0.1131 \pm 0.0006(exp). \tag{4.10}$$

Figure 4.8 illustrates the better agreement between the two parabolae; results, as

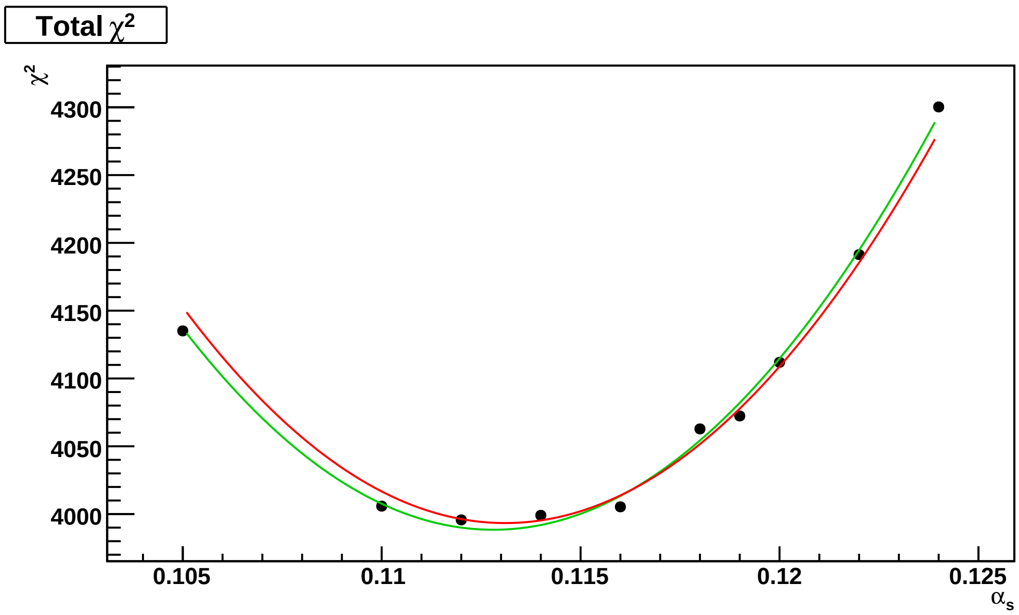

Figure 4.8: $\chi^2(\alpha_s)$ for NNPDF 2.0, recalculated with cuts.

expected, have not changed much and this is a mark of the stability of our procedure. Our final result shall be the estimation 4.9, as this value, according to the analysis of chapter 3, is supposed to be the best for small fluctuations.

Note that in adding DY and JET data the parabola, which had widened from the NNPDF 1.2 case because of not self-consistent observables removal, has got narrower again. The χ^2 has risen again as it should have, but its normalized value, which for the minimum takes the value of 1.17, is approximately constant: no further self-contradicting source has been introduced while adding new experiments. Accordingly with such a gain in available information the experimental error is found to be smaller.

Finally, we may look at how well each experiment is reconstructed by the parton distribution functions for a certain value of α_s. As it has now become usual, the graphs for experiment are displayed in figure 4.9. The PDF best estimates have changed much indeed (see reference [2]), and this is reflected e.g. in the transformation undergone by the HERAI-AV goodeness of fit trend, which now steadily goes up for weak coupling constant values. Even more interesting than these single graphs,

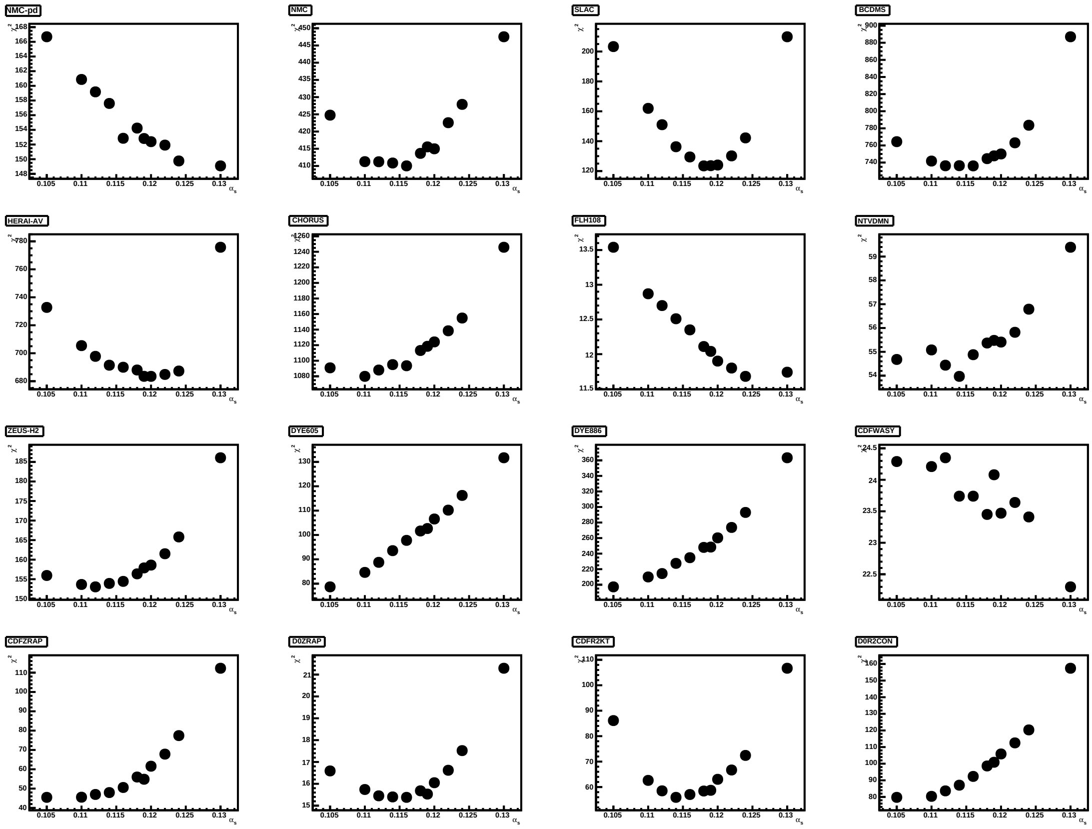

Figure 4.9: $\chi^2(\alpha_s)$ for experiment including DIS, DY and JET data sources.

however, is a plot where all the experiments of a single class are drawn together, diaplayed in figure 4.10. In order to make the image easier to read:

- all graphs have been vertically translated to set their lowest point to zero;
- as differences are the quantities that matter most, the scale has been set equal for all lines to allow a simple comparison;
- points for $\alpha_s = 0.130$ have not been drawn, as they would have made graphs strongly asymmetric and would have needed a strong reduction in vertical scales to be drawn.

The figure actually suggests that for small α_s it is mainly because of deep inelastic scattering bad-fitting that the χ^2 function goes up, forbidding lower estimations of the strong coupling. On the other hand, Drell-Yan data sets experience a dramatical worsening of their description for high α_s values, while they look well-interpolated enough even for the most leftwards points. Everything leads to think that, when these different experiments are fitted together for low values of our constant, the structure of parton distribution functions is mainly determined according to Drell-Yan information, and the action of DIS sets is limited to disagreement. Hadron

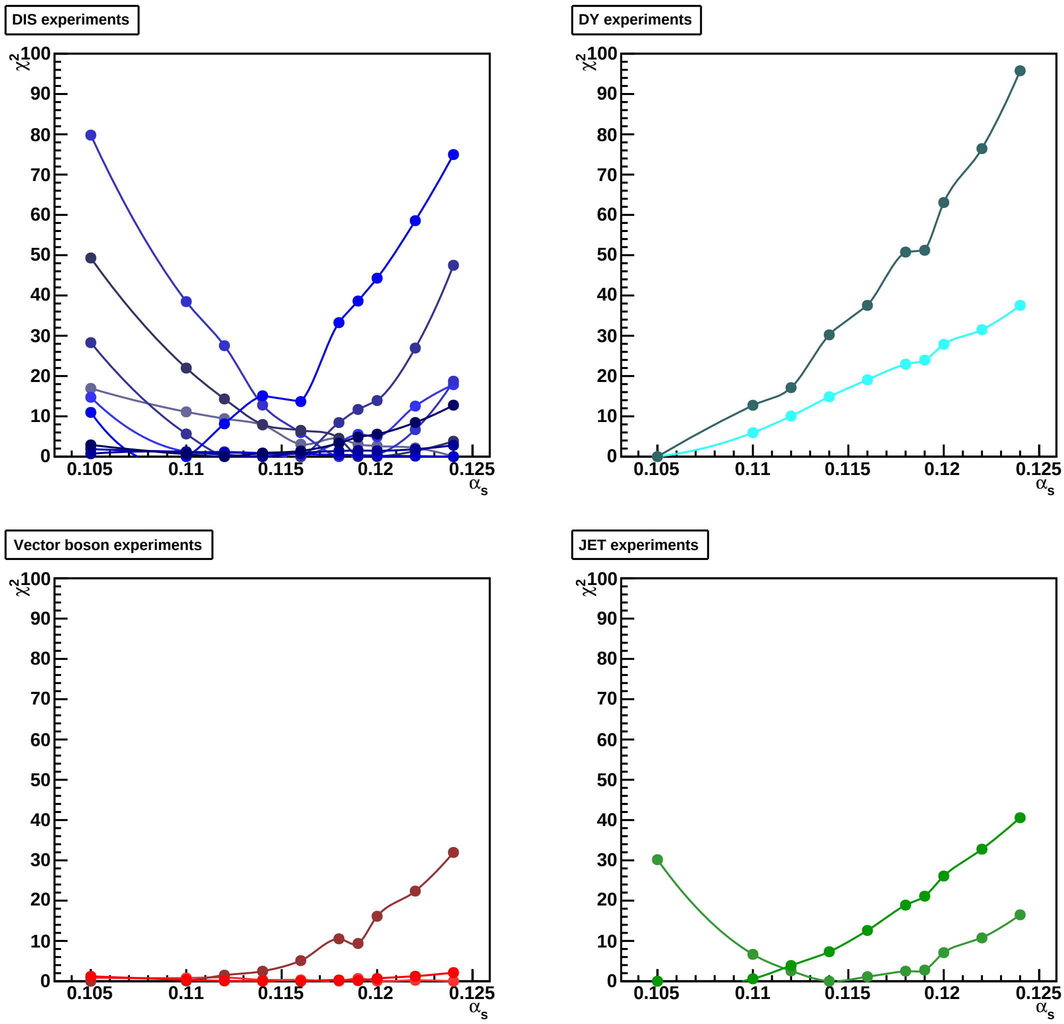

Figure 4.10: $\chi^2(\alpha_s)$ for experiment, collected for data source.

jet inclusive experiments look a little more well-balanced as far as fitting quality is concerned, while vector boson production data sets show only a feeble sensitivity to different values of the strong coupling, even considered that their number of points is quite low.

4.4 Variations with the number of replicas

Some last interesting observations may be made by looking at how results change with the number of replicas used. Indeed in the case of the widest experiment set it has been possible to check the outcomes every time that five new replicas were added, starting from an initial number of 10.

Let us look first at two exaple graphs, collected in figure 4.11 which illustrate the behaviour of fluctuations, i.e. the trend of a χ^2 value for fixed α_s when N_{rep} is gradually increased. Now, *a posteriori*, we can have an idea of what fluctuations

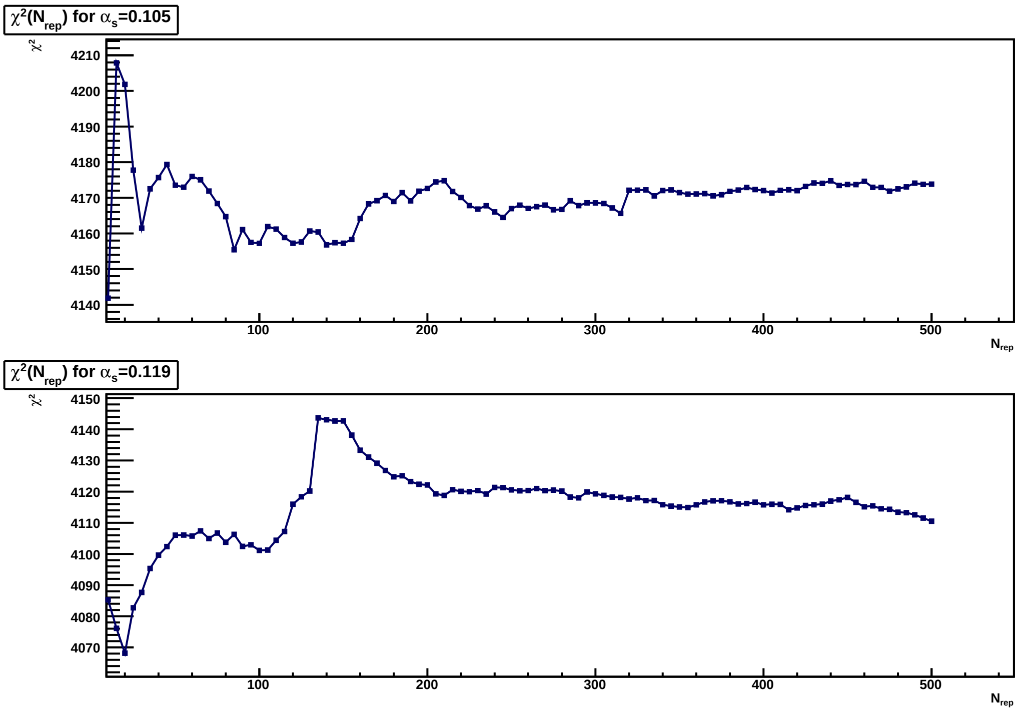

Figure 4.11: Two sample graphs for the trend of χ^2 with the number of replicas.

actually cause: the values of χ^2 perform some kind of random walk in an envelope which gets smaller and smaller around the true value as the number of replicas is increased. Remembering that the prediction for boundaries width implies an inverse proportionality to the square root of N_{rep}, the strong reduction of such an imaginary uncertainty at the beginning and the slackening of the convergence speed towards the right side of the figure are not unexpected.

More interesting yet is the case of the plot of the strong coupling estimate with the least squares method as a function of the number of replicas, which is displayed in image number 4.12. From this graph we may see that, while in the beginning the final value for α_s is quite uncertain, it grows more and more stable as the number of replicas increases. The convergence speed is indeed remarkable if we consider that the constant never goes far than 0.001 from its final value, and such a strenght may be due to the use of many points whose accidental fluctuations are independent. It is possible to argue that the confidence for the esteem of α_s with N_{rep} replicas being inside a certain interval from its asymptotic value may be deduced from this trend. For this purpose the comparison of our case with situations often arising in finance suggests the usage of a volatility parameter, which at a certain time is equal to the standard deviation of the values taken by the considered quantity during a fixed lapse of time before the chosen instant. This estimator, used on a basis of 50 replicas,

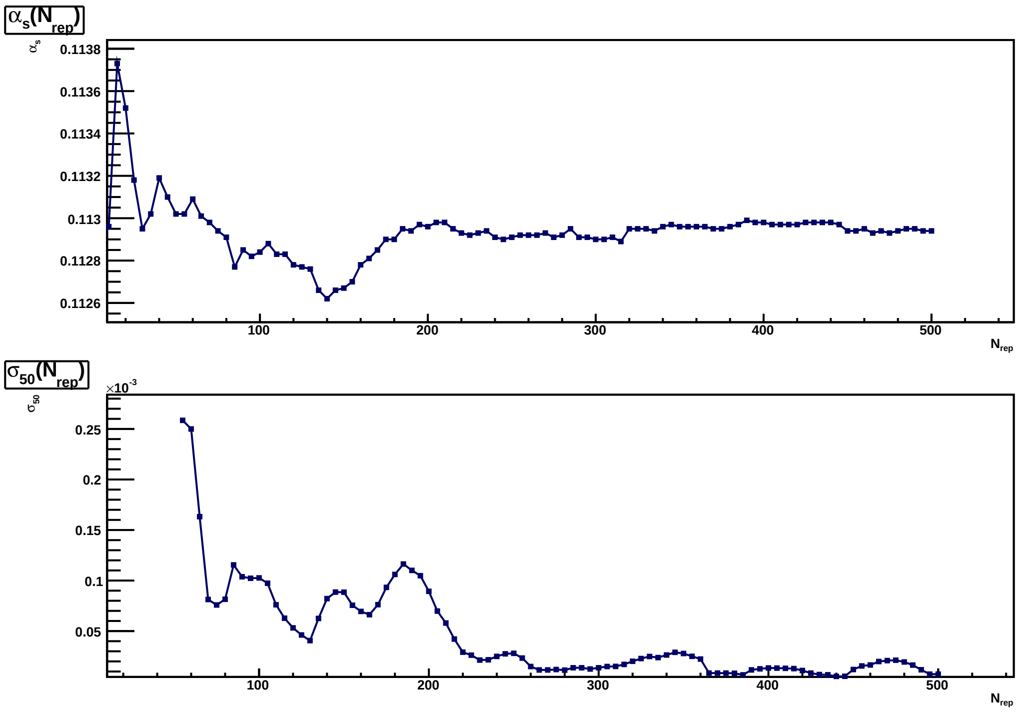

Figure 4.12: α_s best estimate variation with the number of replicas and its volatility.

is plotted below the graph for α_s; the graph shows that the volatility of the strong coupling due to fluctuations, though bouncing a little, decreases as more replicas are added. From this analysis we get confidence enough to state that α_s will not go further from its estimation with 500 replicas than the value taken by its volatility at its last, strong peak before a steady downfall. Being rather pessimistic, we take as a statistical uncertainty the approximate value of the maximum of volatility around $N_{rep} \approx 200$, that is

$$\sigma_{stat} = 0.0001. \tag{4.11}$$

Chapter 5

Conclusions and outlook

We have found that, in reproducing the correct behaviour of a function underlying a point set affected by fluctuations the least squares method is usually the safest and most accurate. However, in the case of high fluctuations and good symmetry of the point set, applying the three points method with cuts results in more reliable outcomes.

Concerning the determination of α_s, we have found the value as an outcome of the NNPDF 1.2 analysis, but its comparison with a study based on the same DIS sources and performed with NNPDF 2.0 has shown that the former result is unreliable because of some faults in the older release of the fitting program. The estimation produced by including Drell-Yan, vector boson production and jet inclusive data as well as deep inelastic scattering experiments in the global fit is

$$\alpha_s = 0.1128 \pm 0.0006^{(exp)} \pm 0.0001^{(stat)}.$$

This outcome is close to the DIS-only value, and yet more precise because it has a wider empirical basis. The statistical uncertainty has been estimated by observing changes in the α_s estimation with the number of replicas used to obtain it.

However, a better solution for the determination of the statistical uncertainty arises because we now have an idea for a possible computation of error bars upon χ^2. The problem in finding confidence level intervals around the chi square found value starting from the distribution of the same quantity for each replica is that the final value of χ^2 is not the average of the single-replica χ^2s, but rather the value obtained computing the same function for the average PDF. These two operations do not commute, as the reconstruction of observables is a highly non-linear procedure. Thus informations for different numbers of replicas are qualitatively very unlike one another when the said numbers are not close. When the replicas sets include e.g. more than one hundred replicas each and a single replica separates them, the chi squares estimations they lead to cannot be that much different. This feature becomes interesting when it is put together with the idea of the jackknife method The latter prescribes error computation for some kind of average of n quantities as the standard deviation of the n values obtained excluding one element at a time, multiplied by $\sqrt{n}$ in order to avoid the underestimation that comes from subsets' strong correlation. The combination of these two strategies could allow for a good estimation of uncertainties and then, because of this appropriate treatment of fluctuations, for the application of more reliable, simple fitting techniques.

Another open question which needs an answer is the relationship of the two suggested three-points methods' estimations for the statistical error on α_s with the width of the probability distribution functions obtained through the toy program; such a direct connection has indeed been looked for, but it has not been found yet.

A possible future development has to do with the mentioned conjectures which hint for a possible problem with low Q^2, low x data. An interesting step in the direction of understanding this problem could be the application of kinematic cuts in that zone and the study of consequences upon the best α_s value.

Last we shall say that in the meanwhile a new version of NNPDF, number 2.1, has been released. It features an improvement in heavy quark thresholds' handling, and the stability of our result under such a change needs to be checked.

Bibliography

[1] R.D. Ball, L. Del Debbio, S. Forte, A. Guffanti, J.I. Latorre, A. Piccione, J. Rojo, and M. Ubiali, *A determination of parton distributions with faithful uncertainty estimation*, Nuclear Physics B **809** (2009), no. 1-2, 1–63.

[2] R.D. Ball, L. Del Debbio, S. Forte, A. Guffanti, J.I. Latorre, J. Rojo, and M. Ubiali, *A first unbiased global NLO determination of parton distributions and their uncertainties*, arXiv **1002**.

[3] R. Brun and F. Rademakers, *ROOT–An object oriented data analysis framework*, Nuclear Instruments and Methods in Physics Research Section A: Accelerators, Spectrometers, Detectors and Associated Equipment **389** (1997), no. 1-2, 81–86.

[4] G.D. Coughlan and J.E. Dodd, *The ideas of particle physics: an introduction for scientists*, Cambridge Univ Pr, 1991.

[5] G. Cowan, *Statistical data analysis*, Oxford University Press, USA, 1998.

[6] A. Das and T. Ferbel, *Introduction to nuclear and particle physics*, World Scientific Pub Co Inc, 2003.

[7] E. Mariani, *Determination of the strong coupling from an unbiased global parton fit*, Undergraduate Thesis, Milan University (2009).

[8] K. Nakamura and (Particle Data Group), J. Phys. G: Nucl. Part. Phys. **37** (2010).